CHAPTER 17

Antenna Measurements

17.1 INTRODUCTION

In the previous sixteen chapters, analytical methods have been outlined which can be used to analyze, synthesize, and numerically compute the radiation characteristics of antennas. Often many antennas, because of their complex structural configuration and excitation method, cannot be investigated analytically. Although the number of radiators that fall into this category has diminished, because special analytical methods (such as the GTD, Moment Method, Finite-Difference Time-Domain and Finite Element) have been developed during the past few years, there are still a fair number that have not been examined analytically. In addition, experimental results are often needed to validate theoretical data.

As was discussed in Chapter 3, Section 3.8.1, it is usually most convenient to perform antenna measurements with the test antenna in its receiving mode. If the test antenna is reciprocal, the receiving mode characteristics (gain, radiation pattern, etc.) are identical to those transmitted by the antenna. The ideal condition for measuring far-field radiation characteristics then, is the illumination of the test antenna by plane waves: uniform amplitude and phase. Although this ideal condition is not achievable, it can be approximated by separating the test antenna from the illumination source by a large distance on an outdoor range. At large radii, the curvature of the spherical phasefront produced by the source antenna is small over the test antenna aperture. If the separation distance is equal to the inner boundary of the far-field region, $2D^2/\lambda$, then the maximum phase error of the incident field from an ideal plane wave is about $22.5°$, as shown in Figure 17.1. In addition to phasefront curvature due to finite separation distances, reflections from the ground and nearby objects are possible sources of degradation of the test antenna illumination.

Experimental investigations suffer from a number of drawbacks such as:

1. For pattern measurements, the distance to the far-field region ($r > 2D^2/\lambda$) is too long even for outside ranges. It also becomes difficult to keep unwanted reflections from the ground and the surrounding objects below acceptable levels.
2. In many cases, it may be impractical to move the antenna from the operating environment to the measuring site.
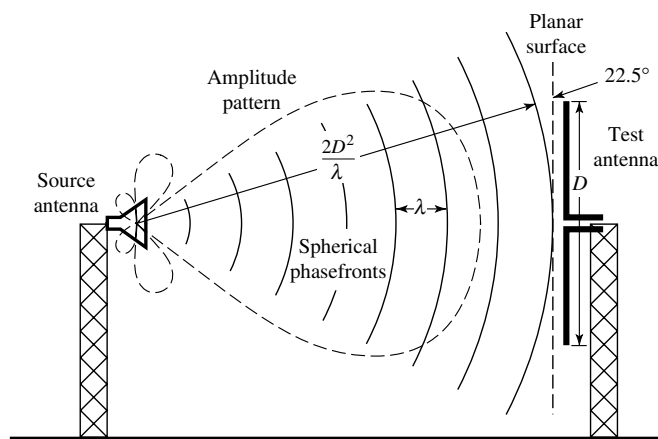
Figure 17.1 Phase error at the edges of a test antenna in the far-field when illuminated by a spherical wave.

3. For some antennas, such as phased arrays, the time required to measure the necessary characteristics may be enormous.

4. Outside measuring systems provide an uncontrolled environment, and they do not possess an all-weather capability.

5. Enclosed measuring systems usually cannot accommodate large antenna systems (such as ships, aircraft, large spacecraft, etc.).

6. Measurement techniques, in general, are expensive.

Some of the above shortcomings can be overcome by using special techniques, such as indoor measurements, far-field pattern prediction from near-field measurements [1]–[4], scale model measurements, and automated commercial equipment specifically designed for antenna measurements and utilizing computer assisted techniques.

Because of the accelerated progress made in aerospace/defense related systems (with increasingly small design margins), more accurate measurement methods were necessary. To accommodate these requirements, improved instrumentation and measuring techniques were developed which include tapered anechoic chambers [5], compact and extrapolation ranges [2], near-field probing techniques [2]–[4], improved polarization techniques and swept-frequency measurements [6], indirect measurements of antenna characteristics, and automated test systems.

The parameters that often best describe an antenna system's performance are the pattern (amplitude and phase), gain, directivity, efficiency, impedance, current distribution, and polarization. Each of these topics will be addressed briefly in this chapter. A more extensive and exhaustive treatment of these and other topics can be found in the *IEEE Standard Test Procedures for Antennas* [7], in a summarized journal paper [8], and in a book on microwave antenna measurements [6]. Most of the material in this chapter is drawn from these three sources. The author recommends that the IEEE publication on test procedures for antennas becomes part of the library of every practicing antenna and microwave engineer.

17.2 ANTENNA RANGES

The testing and evaluation of antennas are performed in antenna ranges. Antenna facilities are categorized as *outdoor* and *indoor* ranges, and limitations are associated with both of them. Outdoor ranges are not protected from environmental conditions whereas indoor facilities are limited by space restrictions. Because some of the antenna characteristics are measured in the receiving mode and require far-field criteria, the ideal field incident upon the test antenna should be a uniform plane wave. To meet this specification, a large space is usually required and it limits the value of indoor facilities.

17.2.1 Reflection Ranges

In general, there are two basic types of antenna ranges: the *reflection* and the *free-space* ranges. The reflection ranges, if judiciously designed [9], can create a constructive interference in the region of the test antenna which is referred to as the "quiet zone." This is accomplished by designing the ranges so that specular reflections from the ground, as shown in Figure 17.2, combine constructively with direct rays.

Usually it is desirable for the illuminating field to have a small and symmetric amplitude taper. This can be achieved by adjusting the transmitting antenna height while maintaining constant that of the receiving antenna. These ranges are of the outdoor type, where the ground is the reflecting surface, and they are usually employed in the UHF region for measurements of patterns of moderately broad antennas. They are also used for systems operating in the UHF to the 16-GHz frequency region.

17.2.2 Free-Space Ranges

Free-space ranges are designed to suppress the contributions from the surrounding environment and include *elevated ranges, slant ranges* [10], *anechoic chambers, compact ranges* [2], and *near-field ranges* [4].
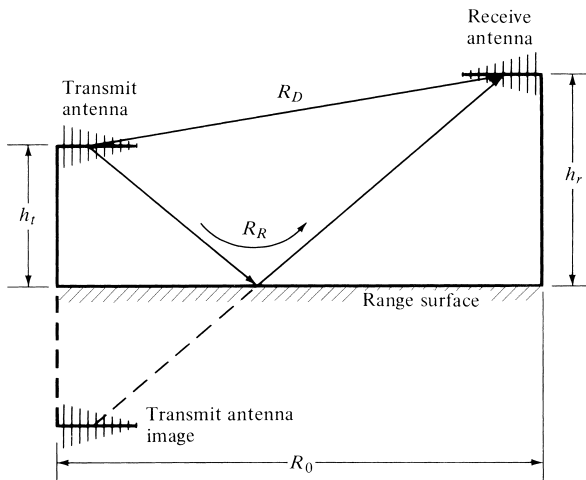

Figure 17.2 Geometrical arrangement for reflection range. (SOURCE: L. H. Hemming and R. A. Heaton, "Antenna Gain Calibration on a Ground Reflection Range," *IEEE Trans. Antennas Propagat.*, Vol. AP-21, No. 4, pp. 532–537, July 1973. © (1973) IEEE)
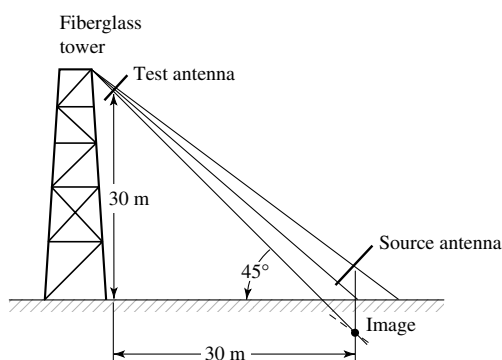
A. Elevated Ranges

Elevated ranges are usually designed to operate mostly over smooth terrains. The antennas are mounted on towers or roofs of adjacent buildings. These ranges are used to test physically large antennas. A geometrical configuration is shown in Figure 17.3(a). The contributions from the surrounding environment are usually reduced or eliminated by [7]

1. carefully selecting the directivity and side lobe level of the source antenna
2. clearing the line-of-sight between the antennas
3. redirecting or absorbing any energy that is reflected from the range surface and/or from any obstacles that cannot be removed
4. utilizing special signal-processing techniques such as modulation tagging of the desired signal or by using short pulses

In some applications, such as between adjacent mountains or hilltops, the ground terrain may be irregular. For these cases, it is more difficult to locate the specular
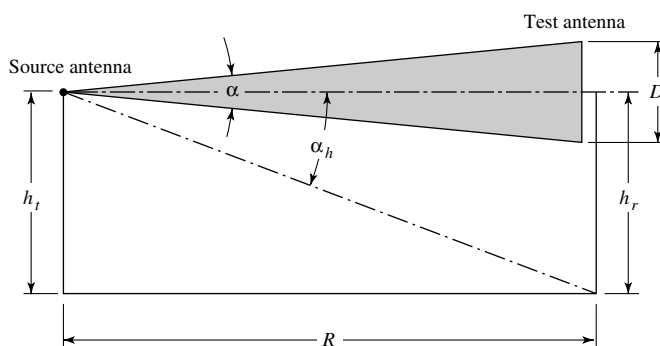
(a) Elevated (after [7])

(b) Slant (after P. W. Arnold [10])

Figure 17.3   Geometries of elevated and slant ranges. (SOURCES: *IEEE Standard Test Procedures for Antennas*, IEEE Std 149–1979, published by IEEE, Inc., 1979, distributed by Wiley; and P. W. Arnold, "The 'Slant' Antenna Range," *IEEE Trans. Antennas Propagat.*, Vol. AP-14, No. 5, pp. 658–659, September 1966. © (1966) IEEE).

reflection points (points that reflect energy toward the test antenna). To take into account the irregular surface, scaled drawings of the vertical profile of the range are usually constructed from data obtained from the U.S. Geological Survey. The maps show ground contours [11], and they give sufficient details which can be used to locate the specular reflection points, determine the level of energy reflected toward the test antenna, and make corrections if it is excessive.

B. Slant Ranges

Slant ranges [10] are designed so that the test antenna, along with its positioner, are mounted at a fixed height on a nonconducting tower while the source (transmitting) antenna is placed near the ground, as shown in Figure 17.3(b). The source antenna is positioned so that the pattern maximum, of its free-space radiation, is oriented toward the center of the test antenna. The first null is usually directed toward the ground specular reflection point to suppress reflected signals. Slant ranges, in general, are more compact than elevated ranges in that they require less land.

C. Anechoic Chambers

To provide a controlled environment, an all-weather capability, and security, and to minimize electromagnetic interference, indoor anechoic chambers have been developed as an alternative to outdoor testing. By this method, the testing is performed inside a chamber having walls that are covered with RF absorbers. The availability of commercial high-quality RF absorbing material, with improved electrical characteristics, has provided the impetus for the development and proliferation of anechoic chambers. Anechoic chambers are mostly utilized in the microwave region, but materials have been developed [12] which provide a reflection coefficient of −40 dB at normal incidence at frequencies as low as 100 MHz. In general, as the operating frequency is lowered, the thickness of RF absorbing material must be increased to maintain a given level of reflectivity performance. An RF absorber that meets the minimum electrical requirements at the lower frequencies usually possesses improved performance at higher frequencies.

Presently there are two basic types of anechoic chamber designs: the *rectangular* and the *tapered chamber*. The design of each is based on geometrical optics techniques, and each attempts to reduce or to minimize specular reflections. The geometrical configuration of each, with specular reflection points depicted, is shown in Figures 17.4(a) and 17.4(b).

The rectangular chamber [13] is usually designed to simulate free-space conditions and maximize the volume of the quiet zone. The design takes into account the pattern and location of the source, the frequency of operation, and it assumes that the receiving antenna at the test point is isotropic. Reflected energy is minimized by the use of high-quality RF absorbers. Despite the use of RF absorbing material, significant specular reflections can occur, especially at large angles of incidence.

Tapered anechoic chambers [14] take the form of a pyramidal horn. They begin with a tapered chamber which leads to a rectangular configuration at the test region, as shown in Figure 17.4(b). At the lower end of the frequency band at which the chamber is designed, the source is usually placed near the apex so that the reflections from the side walls, which contribute to the illuminating fields in the region of the test antenna, occur near the source antenna. For such paths, the phase difference between the direct radiation and that reflected from the walls near the source can be made very small by
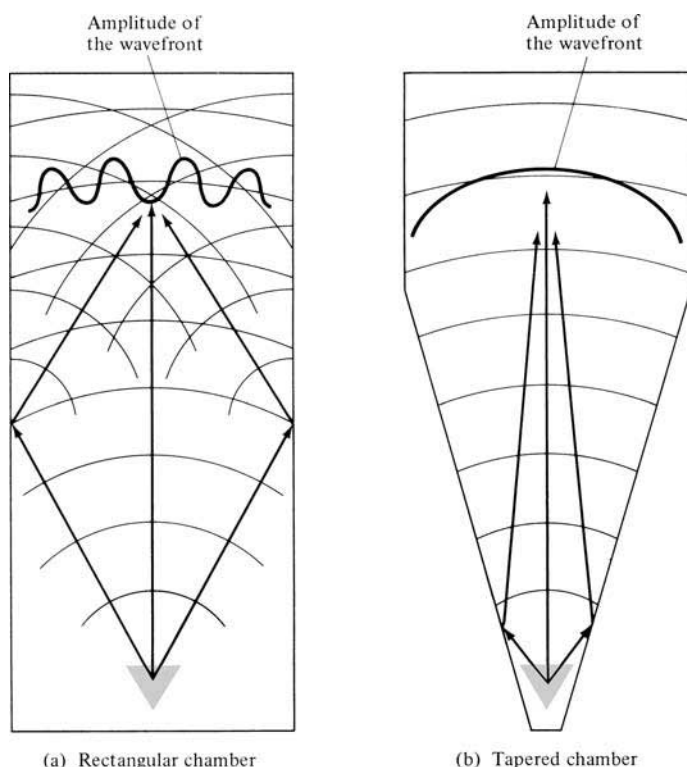
Figure 17.4   Rectangular and tapered anechoic chambers and the corresponding side-wall specular reflections. (SOURCE: W. H. Kummer and E. S. Gillespie, "Antenna Measurements—1978," *Proc. IEEE*, Vol. 66, No. 4, pp. 483–507, April 1978. © (1978) IEEE)

properly locating the source antenna near the apex. Thus the direct and reflected rays near the test antenna region add vectorially and provide a relatively smooth amplitude illumination taper. This can be illustrated by ray-tracing techniques.

As the frequency of operation increases, it becomes increasingly difficult to place the source sufficiently close to the apex that the phase difference between the direct and specularly reflected rays can be maintained below an acceptable level. For such applications, reflections from the walls of the chamber are suppressed by using high-gain source antennas whose radiation toward the walls is minimal. In addition, the source is moved away from the apex, and it is placed closer to the end of the tapering section so as to simulate a rectangular chamber.

17.2.3   Compact Ranges

Microwave antenna measurements require that the radiator under test be illuminated by a uniform plane wave. This is usually achieved only in the far-field region, which in many cases dictates very large distances. The requirement of an ideal plane wave illumination can be nearly achieved by utilizing a compact range.

A *C*ompact *A*ntenna *T*est *R*ange (CATR) is a collimating device which generates nearly planar wavefronts in a very short distance (typically 10–20 meters) compared

to the $2D^2/\lambda$ (minimum) distance required to produce the same size test region using the standard system configuration of testing shown in Figure 17.1. Some attempts have been made to use dielectric lenses as collimators [15], but generally the name compact antenna test range refers to one or more curved metal reflectors which perform the collimating function. Compact antenna test ranges are essentially very large reflector antennas designed to optimize the planar characteristics of the fields in the near field of the aperture. Compact range configurations are often designated according to their analogous reflector antenna configurations: parabolic, Cassegrain, Gregorian, and so forth.

One compact range configuration is that shown in Figure 17.5 where a source antenna is used as an offset feed that illuminates a paraboloidal reflector, which converts the impinging spherical waves to plane waves [2]. Geometrical Optics (GO) is used in Figure 17.5 to illustrate general CATR operation. The rays from a feed antenna can, over the main beam, be viewed as emanating from a point at its phase center. When the phase center of the feed is located at the prime focus of a parabolic reflector, all rays that are reflected by the reflector and arrive at a plane transverse to the axis of the parabola have traveled an equal distance. See Chapter 15, Section 15.4 for details. Therefore, the field at the aperture of the reflector has a uniform phase; i.e., that of a plane wave. In addition to Geometrical Optics, analysis and design of CATRs have been performed with a number of other analytical methods. Compact range test zone fields have been predicted by the Method of Moments (MoM), but at high frequencies, the large electrical size of the CATR system makes the use of MoM, Finite-Difference Time-Domain (FD-TD), and Finite Element Method (FEM) impractical. High-frequency techniques, however, are well suited for compact range analysis because the fields of interest are near the specular reflection direction, and the reflector is electrically large. The Geometrical Theory of Diffraction (GTD) is, in principle, an appropriate technique, but it is difficult to implement for serrated-edge reflectors due to the large number of diffracting edges. To date, Physical Optics (PO) is probably the most practical and efficient method of predicting the performance of CATRs [16], [17].

The major drawbacks of compact ranges are aperture blockage, direct radiation from the source to the test antenna, diffractions from the edges of the reflector and
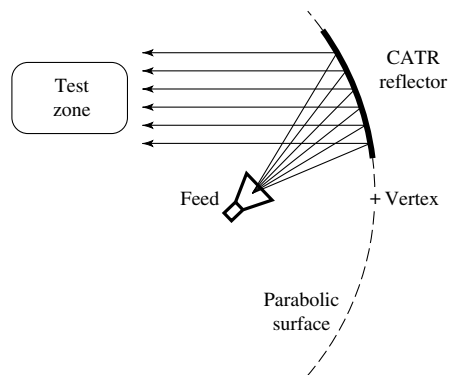

Figure 17.5   A Compact Antenna Test Range (CATR) synthesizes planar phase fronts by collimating spherical waves with a section of paraboloidal reflector.

feed support, depolarization coupling between the two antennas, and wall reflections. The use of an offset feed eliminates aperture blockage and reduces diffractions. Direct radiation and diffractions can be reduced further if a reflector with a long focal length is chosen. With such a reflector, the feed can then be mounted below the test antenna and the depolarization effects associated with curved surfaces are reduced. Undesirable radiation toward the test antenna can also be minimized by the use of high-quality absorbing material. These and other concerns will be discussed briefly.

A. CATR Performance

A perfect plane wave would be produced by a CATR if the reflector has an ideal parabolic curvature, is infinite in size and is fed by a point source located at its focus. Of course CATR reflectors are of finite size, and their surfaces have imperfections; thus the test zone fields they produce can only approximate plane waves. Although there are different configurations of CATR, their test zone fields have some common characteristics. The usable portion of the test zone consists of nearly planar wavefronts and is referred to as the "quiet zone." Outside the quiet zone, the amplitude of the fields decreases rapidly as a function of distance transverse to the range axis. The size of the quiet zone is typically about 50%–60% of the dimensions of the main reflector. Although the electromagnetic field in the quiet zone is often a very good approximation, it is not a "perfect" plane wave. The imperfections of the fields in the quiet zone from an ideal plane wave are usually represented by phase errors, and ripple and taper amplitude components. These discrepancies from an ideal plane wave, that occur over a specified test zone dimension, are the primary figures of merit of CATRs. For most applications phase deviations of less than $10°$, peak-to-peak amplitude ripples of less than 1 dB, and amplitude tapers of less than 1 dB are considered adequate. More stringent quiet-zone specifications may be required to measure, within acceptable error levels, low-side lobe antennas and low-observable scatterers. The sources of quiet-zone taper and ripple are well known, but their minimization is a source of much debate.

Amplitude taper across the quiet zone can be attributed to two sources: the feed pattern and space-attenuation. That portion of the radiation pattern of the feed antenna which illuminates the CATR reflector is directly mirrored into the quiet zone. For example, if the 3-dB beamwidth of the feed is equal to about 60% of the angle formed by lines from the reflector edges to the focal point, then the feed will contribute 3 dB of quiet-zone amplitude taper. In general, as the directivity of the feed antenna increases, quiet-zone amplitude taper increases. Usually, low-gain feed antennas are designed to add less than a few tenths of a dB of amplitude taper. The $1/r^2$ space-attenuation occurs with the spherical spreading of the uncollimated radiation from the feed. Although the total path from the feed to the quiet zone is a constant, the distance from the feed to the reflector varies. These differences in the propagation distances from the feed to various points across the reflector surface cause amplitude taper in the quiet zone due to space-attenuation. This taper is asymmetric in the plane of the feed offset.

Amplitude and phase ripple are primarily caused by diffractions from the edges of the reflector. The diffracted fields are spread in all directions which, along with the specular reflected signal, form constructive and destructive interference patterns in the quiet zone, as shown in Figure 17.6(a). Considerable research has been done on reflector edge terminations in an effort to minimize quiet-zone ripple. Reflector edge treatments are the physical analogs of windowing functions used in Fourier transforms.
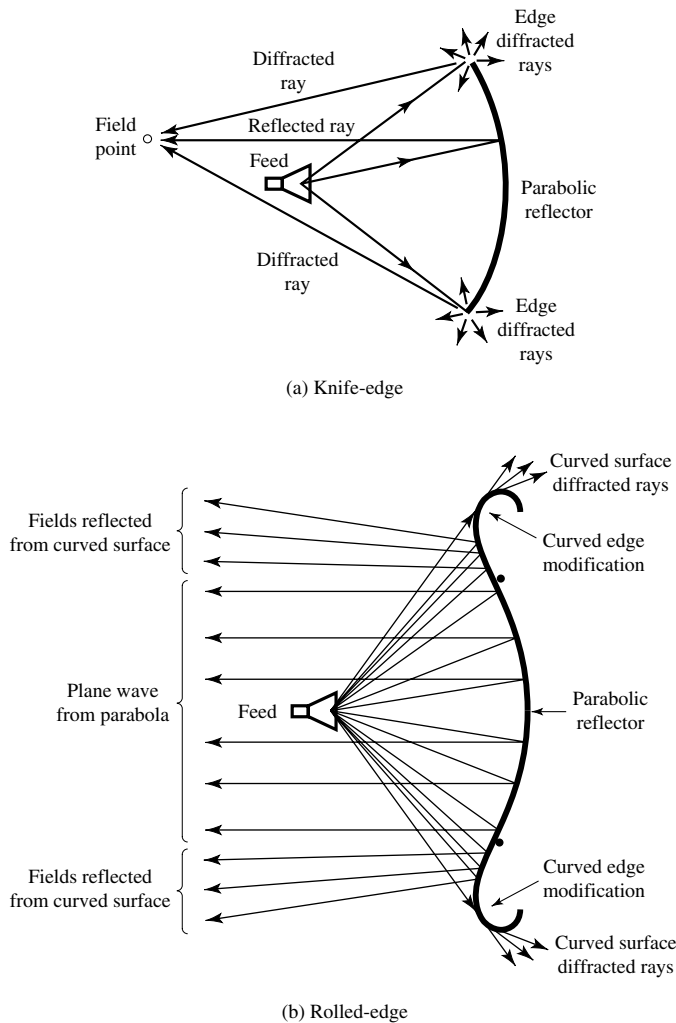
(a) Knife-edge

(b) Rolled-edge

Figure 17.6 Amplitude and phase ripple in the quiet-zone fields produced by a compact antenna test range caused by the phasor sum of the reflected and diffracted rays from the reflector. (SOURCE: W. D. Burnside, M. C. Gilreath, B. M. Kent and G. L. Clerici, "Curved Edge Modification of Compact Range Reflectors," *IEEE Trans. Antennas Propagat.*, Vol. AP-35, No. 2, pp. 176–182, February 1987. © (1987) IEEE)

Edge treatments reduce the discontinuity of the reflector/free-space boundary, caused by the finite size of the reflector, by providing a gradually tapered transition. Common reflector edge treatments include serrations and rolled edges, as shown in Figure 17.7(a, b). The serrated edge of a reflector tapers the amplitude of the reflected fields near the edge. An alternate interpretation of the effects of serrations is based on edge diffraction. Serrations produce many low-amplitude diffractions as opposed to, for example, the large-amplitude diffractions that would be generated by the four straight edges and corners of a rectangular knife-edged reflector. These small diffractions are quasi-randomized in location and direction; hence, they are likely to have cancellations in the
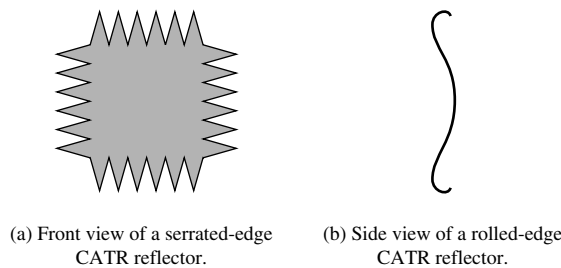
(a) Front view of a serrated-edge
CATR reflector.

(b) Side view of a rolled-edge
CATR reflector.

Figure 17.7   Two common CATR reflector edge treatments that are used to reduce the diffracted fields in the quiet zone.

quiet zone. Although most serrated-edge CATRs have triangular serrations, curving the edges of each serration can result in improved performance at high frequencies [18]. A number of blended, rolled-edge treatments have been suggested as alternatives to serrations, and have been implemented to gradually redirect energy away from the quiet zone, as shown in Figure 17.6(b) [19]–[21]. In these designs, the concave parabolic surface of the reflector is blended into a convex surface which wraps around the edges of the reflector and terminates behind it. The predicted quiet-zone fields produced by a knife-edged reflector compared to those produced by a rolled-edged reflector are shown, respectively, in Figures 17.8(a,b) and demonstrate the effectiveness of this edge treatment. Another method of reducing quiet-zone ripple is to taper the illumination amplitude near the reflector edges. This can be accomplished with a high-gain feed or the feed can consist of an array of small elements designed so that a null in the feed pattern occurs at the reflector edges [22]–[25]. Finally, the surface currents on the reflector can be terminated gradually at the edges by tapering the conductivity and/or the impedance of the reflector via the application of lossy material.

The frequency of operation of a CATR is determined by the size of the reflector and its surface accuracy. The low-frequency limit is usually encountered when the reflector is about 25 to 30 wavelengths in diameter [26]. Quiet-zone ripple becomes large at the low-frequency limit. At high frequencies, reflector surface imperfections contribute to the quiet-zone ripple. A rule of thumb used in the design of CATRs is that the surface must deviate less than about 0.007λ from that of a true paraboloid [27]. Since the effects of reflector surface imperfections are additive, dual reflector systems must maintain twice the surface precision of a single reflector system to operate at the same frequency. Many CATR systems operate typically from 1 GHz to 100 GHz.

B. CATR Designs

Four reflector configurations that have been commercially developed will be briefly discussed: *the single paraboloid, the dual parabolic-cylinder, the dual shaped-reflector*, and *the single parabolic-cylinder systems*. The first three configurations are relatively common fully collimating compact ranges; the fourth is a hybrid approach which combines aspects of compact range technology with near-field/far-field (NF/FF) techniques.

The single paraboloidal reflector CATR design was illustrated in Figure 17.5. As with all compact range designs, the feed antenna is offset by some angle from the propagation direction of the collimated energy. This is done to eliminate blockage and to reduce scattering of the collimated fields by the feed. To achieve this offset, the reflector is a sector of a paraboloid that does not include the vertex. This design is
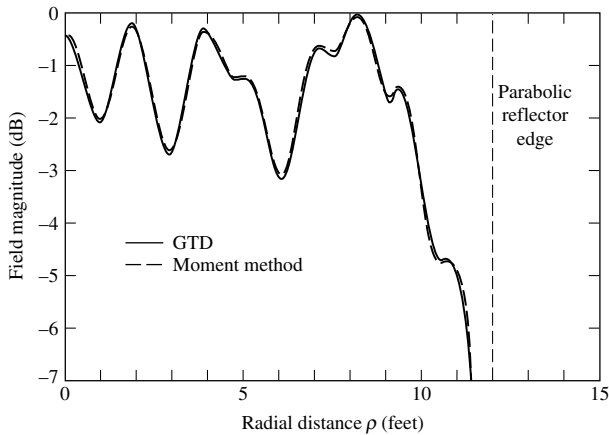
(a) Knife-edge
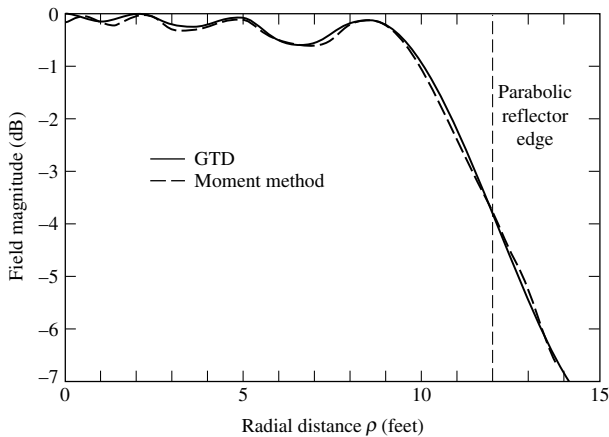
(b) Rolled-edge

Figure 17.8   Predicted quiet-zone field amplitude versus transverse distance for knife-edge and rolled-edge reflectors. (SOURCE: W. D. Burnside, M. C. Gilreath, B. M. Kent, and G. L. Clerici, "Curved Edge Modification of Compact Range Reflectors," *IEEE Trans. Antennas Propagat.*, Vol. AP-35, No. 2, pp. 176–182, February 1987. © (1987) IEEE)

referred to as a "*virtual vertex*" compact range. With only one reflector, the paraboloidal CATR has a minimum number of surfaces and edges that can be sources of quiet-zone ripple. Feed spillover into the quiet zone is also low with this design since the feed antenna is pointed almost directly away from the test zone. On the other hand, it is more difficult and costly to produce a high-precision surface that is curved in two planes (three-dimensional) compared to producing a reflector that is curved in only one plane (two-dimensional). In addition, it has been reported that the single paraboloidal reflector design depolarizes the incident fields to a greater degree than other CATR designs. This is due to the relatively low *f/d* ratio needed to simultaneously maintain the feed antenna between the test zone and the reflector while keeping the test zone as close as possible to the reflector aperture [28].
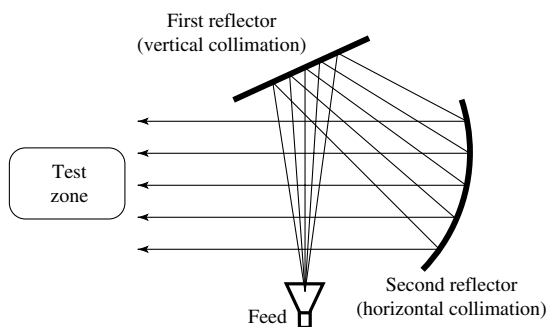
Figure 17.9   Dual parabolic-cylinder compact range collimates the fields in one plane with first reflector and then collimates the fields in the orthogonal plane with second reflector.

The dual parabolic-cylinder reflector concept is illustrated in Figure 17.9, and it consists of two parabolic cylinders arranged so that one is curved in one plane (vertical or horizontal) while the other is curved in the orthogonal plane. The spherical phase fronts radiated by the feed antenna are collimated first in the horizontal or vertical plane by the first reflector, then are collimated in the orthogonal plane by the second reflector [29]. Because the boresight of the feed antenna is directed at almost 90° to the plane wave propagation direction, direct illumination of the test zone by the feed can be relatively high. In practice, quiet-zone contamination from feed spillover is virtually eliminated through the use of range gating. Relatively low cross polarization is produced with this design because the doubly folded optics results in a long focal length main reflector.

The dual shaped-reflector CATR, shown schematically in Figure 17.10, is similar in design to a Cassegrain antenna, but the reflector surfaces are altered from the classical parabolic/hyperbolic shapes. An iterative design process is used to determine the shapes of the subreflector and main reflector needed to yield the desired quiet-zone performance. The shape of the subreflector maps the high-gain feed pattern into a nearly optimum illumination of the main reflector. An almost uniform energy density illuminates the central part of the main reflector while the amplitude tapers toward the reflector edges. This design results in a very high illumination efficiency (the power of the collimated quiet-zone fields relative to the system input power) [30]. Two of the consequences of this high illumination efficiency are (1) the reduction of spillover into the chamber reduces range clutter, and (2) the increased RF power delivered to the target increases system sensitivity.
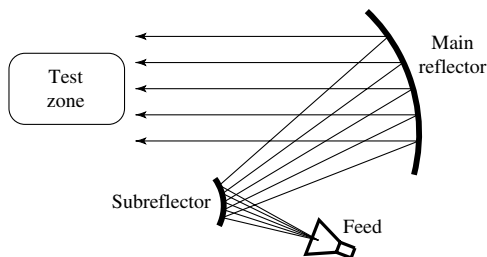

Figure 17.10   Dual shaped-reflector compact range analogous to a Cassegrain system.
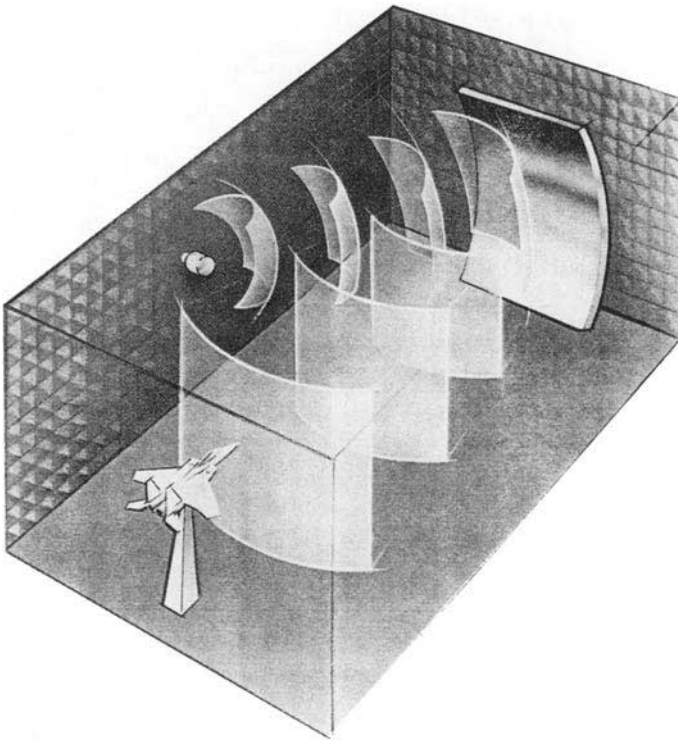
Figure 17.11 ASU Single-Plane Collimating Range (SPCR) produces a cylindrical wave in the quiet zone (artist rendering by Michael Hagelberg).

The single parabolic-cylinder reflector system is essentially half of the dual parabolic-cylinder CATR. The reflector has a parabolic curvature in the vertical plane and is flat in the horizontal plane. This semicompact antenna test range collimates the fields only in the vertical plane, producing a quiet zone which consists of cylindrical waves, as shown in Figure 17.11 [31]–[33]. Such a compact range configuration is utilized in the ElectroMagnetic Anechoic Chamber (EMAC) at Arizona State University [32], [33].

This *Single-Plane Collimating Range* (SPCR) approach results in a number of advantages and compromises compared to conventional CATR systems and near-field/far-field (NF/FF) systems. For antennas that are small compared to the curvature of the cylindrical phasefront, far-field radiation patterns can be measured directly. Because of the folded optics, the radius of the cylindrical phasefront produced by the SPCR is larger than the radius of the spherical phasefront obtainable by separating the source antenna from the test antenna in a direct illumination configuration within the same anechoic chamber. Thus, with the SPCR it is possible to measure, directly, the far-field patterns of larger antennas compared to those directly measurable on an indoor far-field range. When the size of the antenna is significant relative to the curvature of the cylindrical phasefront, a NF/FF transformation is used to obtain the far-field pattern. However, because the fields are collimated in the vertical plane, only a one-dimensional transformation is required. This greatly simplifies the transformation algorithm. Most

importantly, there is a one-to-one correlation between a single azimuthal pattern cut measured in the near-field, and the predicted far-field pattern. The data acquisition time is identical to that of conventional CATRs, and the NF/FF calculation time is nearly negligible. Another advantage of the SPCR is the size of the quiet zone. In the vertical plane, the quiet-zone dimension compared to the SPCR reflector is similar to that of conventional CATRs (about 50% to 60%). However, in the horizontal plane, the quiet zone is nearly 100% of the horizontal dimension of the reflector. For a given size anechoic chamber and reflector, targets having much larger horizontal dimensions (yaw patterns of aircraft, for example) can be measured using the SPCR than is possible using a conventional CATR. The SPCR system is relatively inexpensive; the manufacturer estimates that its cost is about 60% of conventional CATR systems.

In addition to the added complexity of NF/FF transformation considerations, this cylindrical wave approach has other disadvantages compared to conventional CATR designs. Because the quiet-zone fields are expanding cylindrically as they propagate along the axis of the range, a large portion of the anechoic chamber is directly illuminated. This should be carefully considered in the design of the side walls of the anechoic chamber to control range clutter. Also, some measurement sensitivity is sacrificed for the same reason.

Compact antenna test ranges enable the measurement of full-sized antennas in very short distances, usually within the controlled environment of an anechoic chamber. A compact antenna test range can be used to accomplish any type of antenna testing (including radiation patterns, gain, efficiency, etc.) that can be performed on an outdoor facility.

17.2.4 Near-Field/Far-Field Methods

The dimensions of a conventional test range can be reduced by making measurements in the near-field, and then using analytical methods to transform the measured near-field data to compute the far-field radiation characteristics [2]–[4], [34]. These are referred to as *near-field to far-field (NF/FF)* methods. Such techniques are usually used to measure patterns, and they are often performed indoors. Therefore, they provide a controlled environment and an all-weather capability, the measuring system is time and cost effective, and the computed patterns are as accurate as those measured in a far-field range. However, such methods require more complex and expensive systems, more extensive calibration procedures, more sophisticated computer software, and the patterns are not obtained in real time.

The near-field measured data (usually amplitude and phase distributions) are measured by a scanning field probe over a preselected surface which may be a *plane*, a *cylinder*, or a *sphere*. The measured data are then transformed to the far-field using analytical Fourier transform methods. The complexity of the analytical transformation increases from the planar to the cylindrical, and from the cylindrical to the spherical surfaces. The choice is primarily determined by the antenna to be measured.

In general, the planar system is better suited for high-gain antennas, especially planar phased arrays, and it requires the least amount of computations and no movement of the antenna. Although the cylindrical system requires more computations than the planar, for many antennas its measuring, positioning, and probe equipment are the least expensive. The spherical system requires the most expensive computation, and antenna and probe positioning equipment, which can become quite significant for

large antenna systems. This system is best suited for measurements of low-gain and omnidirectional antennas.

Generally, implementation of NF/FF transformation techniques begins with measuring the magnitude and phase of the tangential electric field components radiated by the test antenna at regular intervals over a well-defined surface in the near field. By the principle of *modal expansion*, the sampled E-field data is used to determine the amplitude and phase of an angular spectrum of plane, cylindrical, or spherical waves. Expressing the total field of the test antenna in terms of a modal expansion, allows the calculation of the field at any distance from the antenna. Solving for the fields at an infinite distance results in the far-field pattern.

A consideration of the general case of scanning with ideal probes over an arbitrary surface [34] reveals that the choice of scanning surfaces is limited. Morse and Feshbach [35] show that derivation of the far-zone vector field from the near-field depends on vector wave functions that are orthogonal to that surface. Planar, circular cylindrical, spherical, elliptic cylindrical, parabolic cylindrical, and conical are the six coordinate systems that support orthogonal vector wave solutions. The first three coordinate systems are conducive to convenient data acquisition, but the last three require scanning on an elliptic cylinder, a parabolic cylinder, or a sphere in conical coordinates [34]. Thus, the three NF/FF techniques that have been developed and are widely used are based on *planar, cylindrical*, and *spherical* near-field scanning surfaces.

Acquisition of planar near-field data is usually conducted over a rectangular x-y grid, as shown in Figure 17.12(a), with a maximum near-field sample spacing of $\Delta x = \Delta y = \lambda/2$ [36]. It is also possible to acquire the near-field measurements on a plane-polar grid [37] or a bipolar grid [38]. The test antenna is held stationary while the probe (typically an open-ended waveguide or small horn) is moved to each grid location on the plane. As the probe location varies, its orientation relative to the test antenna changes, as illustrated in Figure 17.13. This directive property of the probe, as well as its polarization, must be taken into account using the technique of *probe compensation* [3], [4]. Probe compensation methods use the well-known Lorentz reciprocity theorem to couple the far-zone fields of the test antenna to those of the measuring probe.
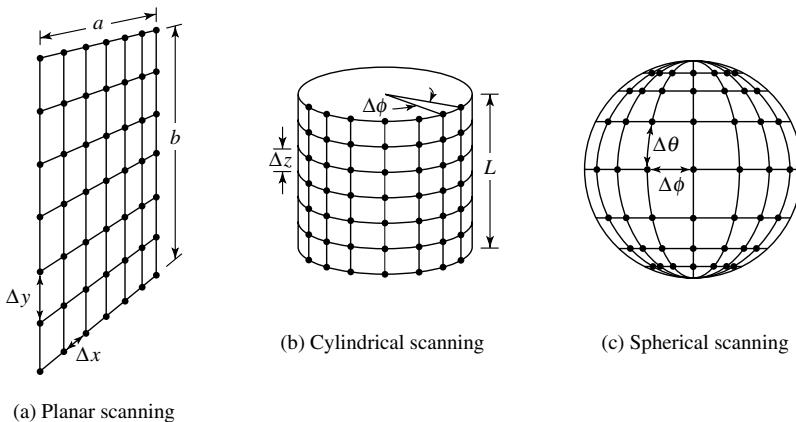

(a) Planar scanning

(b) Cylindrical scanning

(c) Spherical scanning

Figure 17.12 Three near-field scanning surfaces that permit convenient data acquisition (planar, cylindrical, and spherical).
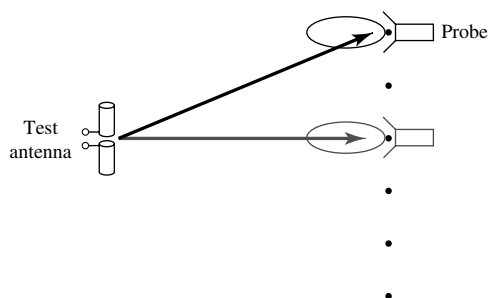
Figure 17.13 Probe compensation of near-field measurements due to nonisotropic radiation pattern of the probe.

The principal advantage of the planar near-field to far-field transformation, over the cylindrical and spherical techniques, is its mathematical simplicity. Furthermore, the planar transformation is suitable for applying the computationally efficient Fast Fourier Transform (FFT) algorithm [39]. Assuming that the number of near-field data points is 2^n (or artificially padded to that number with points of zero value) where n is a positive integer, the full planar far-field transformation can be computed in a time proportional to $(ka)^2 \log_2(ka)$ where a is the radius of the smallest circle that inscribes the test antenna [34]. Planar NF/FF techniques are well suited for measuring antennas which have low backlobes. These include directional antennas such as horns, reflector antennas, planar arrays, and so forth. The primary disadvantage of probing the near-field on a planar surface to calculate the far-field is that the resulting far-field pattern is over a limited angular span. If the planar scanning surface is of infinite extent, one complete hemisphere of the far-field can be computed.

A complete set of near-field measurements over a *cylindrical* surface includes the information needed to compute complete azimuthal patterns for all elevation angles, excluding the conical regions at the top and bottom of the cylinder axis. Since the numerical integrations can be performed with the FFT, the cylindrical transformation exhibits numerical efficiencies and proportional computation times similar to those of the planar transformation. The angular modal expansion, however, is expressed in terms of Hankel functions, which can be more difficult to calculate, especially for large orders.

The cylindrical scanning grid is shown in Figure 17.12(b). The maximum angular and vertical sample spacing is

$$\Delta\phi = \frac{\lambda}{2(a + \lambda)} \tag{17-1}$$

and

$$\Delta z = \lambda/2 \tag{17-2}$$

where λ is the wavelength and a is the radius of the smallest cylinder that encloses the test antenna.

A typical cylindrical scanning system is illustrated in Figure 17.14(a). The azimuthal location of the antenna is held constant while the fields are probed at discrete locations
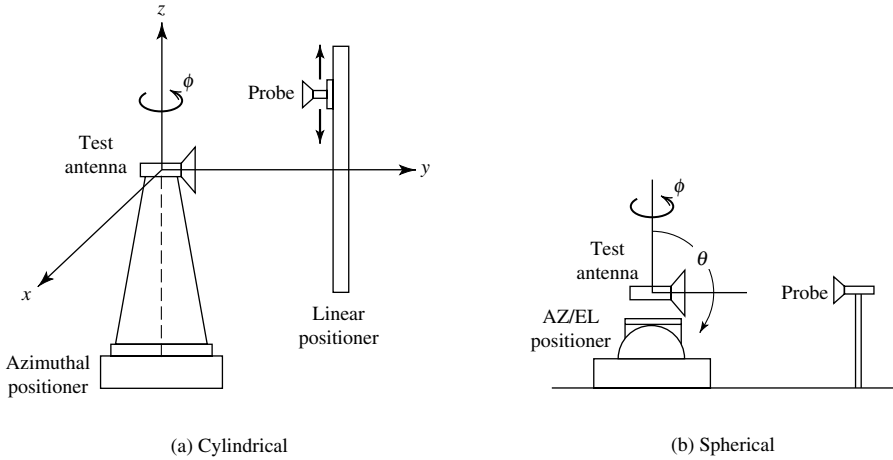
(a) Cylindrical   (b) Spherical

Figure 17.14 Schematic representation of typical cylindrical and spherical surface near-field positioning systems.

in the vertical direction at some fixed distance from the antenna. At the completion of each vertical scan, the test antenna is rotated to the next angular position. The orientation of the probe with respect to the test antenna changes as the vertical location of the probe changes, thus a probe correction is generally required as in the planar case. In addition to directional antennas, the radiation patterns of antennas with narrow patterns along the vertical axis (horizontal fan beam antennas and vertical dipoles for example) can be predicted efficiently with the cylindrical NF/FF technique.

The information obtained by scanning the near-field radiation over a *spherical* surface enclosing a test antenna makes possible the most complete prediction of the far-field radiation pattern. The spherical scanning grid is illustrated in Figure 17.12(c). When sampled at the rate of

$$\Delta\theta = \frac{\lambda}{2(a+\lambda)} \qquad (17\text{-}3)$$

and

$$\Delta\phi = \frac{\lambda}{2(a+\lambda)} \qquad (17\text{-}4)$$

all of the spatial radiation characteristics of the test antenna are included in the transformation. Any far-field pattern cut can be computed from a complete near-field measurement with the spherical scanning scheme. Typically, a spherical scan is accomplished by fixing the location and orientation of the probe and varying the angular orientation of the test antenna with a dual-axis positioner, as shown in Figure 17.14(b). Since the probe is always pointed directly toward the test antenna, probe correction can be neglected for sufficiently large scan radii [34]. However, in general, probe correction is necessary.

The primary drawback of the spherical scanning technique lies in the mathematical transformation. A significant portion of the transformation cannot be accomplished via FFTs. Numerical integrations, matrix operations, and simultaneous solution of equations are required. This increases the computational time and difficulty of the transformation considerably over those of the planar and cylindrical transformations.

A. Modal-Expansion Method for Planar Systems

The mathematical formulations of the planar NF/FF system are based on the plane wave (modal) expansion using Fourier transform (spectral) techniques. Simply stated, any monochromatic, but otherwise arbitrary, wave can be represented as a superposition of plane waves traveling in different directions, with different amplitudes, but all of the same frequency. The objective of the plane wave expansion is to determine the unknown amplitudes and directions of propagation of the plane waves. The results comprise what is referred to as a *modal expansion* of the arbitrary wave. Similarly, cylindrical wave and spherical wave expansions are used to determine far-field patterns from fields measured in the near field over cylindrical and spherical surfaces, respectively.

The relationships between the near-zone E-field measurements and the far-zone fields for planar systems follow from the transform (spectral) techniques of Chapter 12, Section 12.9, represented by (12-73)–(12-75), or

$$\mathbf{E}(x, y, z) = \frac{1}{4\pi^2} \int_{-\infty}^{\infty} \int_{-\infty}^{\infty} \mathbf{f}(k_x, k_y) e^{-j\mathbf{k}\cdot\mathbf{r}} \, dk_x \, dk_y \qquad (17\text{-}5)$$

where

$$\mathbf{f}(k_x, k_y) = \hat{\mathbf{a}}_x f_x(k_x, k_y) + \hat{\mathbf{a}}_y f_y(k_x, k_y) + \hat{\mathbf{a}}_z f_z(k_x, k_y) \qquad (17\text{-}5a)$$

$$\mathbf{k} = \hat{\mathbf{a}}_x k_x + \hat{\mathbf{a}}_y k_y + \hat{\mathbf{a}}_z k_z \qquad (17\text{-}5b)$$

$$\mathbf{r} = \hat{\mathbf{a}}_x x + \hat{\mathbf{a}}_y y + \hat{\mathbf{a}}_z z \qquad (17\text{-}5c)$$

where $\mathbf{f}(k_x, k_y)$ represents the plane wave spectrum of the field. The x and y components of the electric field measured over a plane surface ($z = 0$) from (17-5) are

$$E_{xa}(x, y, z = 0) = \frac{1}{4\pi^2} \int_{-\infty}^{\infty} \int_{-\infty}^{\infty} f_x(k_x, k_y) e^{-j(k_x x + k_y y)} \, dk_x \, dk_y \qquad (17\text{-}6a)$$

$$E_{ya}(x, y, z = 0) = \frac{1}{4\pi^2} \int_{-\infty}^{\infty} \int_{-\infty}^{\infty} f_y(k_x, k_y) e^{-j(k_x x + k_y y)} \, dk_x \, dk_y \qquad (17\text{-}6b)$$

The x and y components of the *plane wave spectrum*, $f_x(k_x, k_y)$ and $f_y(k_x, k_y)$, are determined in terms of the near-zone electric field from the Fourier transforms of (17-6a) and (17-6b) as given by (12-85a), (12-85b), or

$$\boxed{f_x(k_x, k_y) = \int_{-b/2}^{+b/2} \int_{-a/2}^{+a/2} E_{xa}(x', y', z' = 0) e^{+j(k_x x' + k_y y')} \, dx' \, dy'} \qquad (17\text{-}7a)$$

$$\boxed{f_y(k_x, k_y) = \int_{-b/2}^{+b/2} \int_{-a/2}^{+a/2} E_{ya}(x', y', z' = 0) e^{+j(k_x x' + k_y y')} \, dx' \, dy'} \qquad (17\text{-}7b)$$

The far-field pattern of the antenna, in terms of the plane wave spectrum function **f**, is then that of (12-107)

$$\mathbf{E}(r, \theta, \phi) \simeq j\frac{ke^{-jkr}}{2\pi r}[\cos\theta\mathbf{f}(k_x, k_y)]$$ (17-8)

or (12-111)

$$E_\theta(r, \theta, \phi) \simeq j\frac{ke^{-jkr}}{2\pi r}(f_x\cos\phi + f_y\sin\phi)$$ (17-9a)

$$E_\phi(r, \theta, \phi) \simeq j\frac{ke^{-jkr}}{2\pi r}\cos\theta(-f_x\sin\phi + f_y\cos\phi)$$ (17-9b)

The procedure then to determine the far-zone field from near-field measurements is as follows:

1. Measure the electric field components $E_{xa}(x', y', z' = 0)$ and $E_{ya}(x', y', z' = 0)$ in the near field.
2. Find the plane wave spectrum functions f_x and f_y using (17-7a) and (17-7b).
3. Determine the far-zone electric field using (17-8) or (17-9a) and (17-9b).

Similar procedures are used for cylindrical and spherical measuring systems except that the constant surfaces are, respectively, cylinders and spheres. However, their corresponding analytical expressions have different forms.

It is apparent once again, from another application problem, that if the tangential field components are known along a plane, the plane wave spectrum can be found, which in turn permits the evaluation of the field at any point. The computations become more convenient if the evaluation is restricted to the far-field region.

B. Measurements and Computations

The experimental procedure requires that a plane surface, a distance z_0 from the test antenna, be selected where measurements are made as shown in Figure 17.12(a). The distance z_0 should be at least two or three wavelengths away from the test antenna to be out of its reactive near-field region. The plane over which measurements are made is usually divided into a rectangular grid of M × N points spaced Δx and Δy apart and defined by the coordinates $(m\Delta x, n\Delta y, 0)$ where $-M/2 \leq m \leq M/2 - 1$ and $-N/2 \leq n \leq N/2 - 1$. The values of M and N are determined by the linear dimensions of the sampling plane divided by the sampling space. To compute the far-field pattern, it requires that both polarization components of the near field are measured. This can be accomplished by a simple rotation of a linear probe about the longitudinal axis or by the use of a dual-polarized probe. The probe used to make the measurements must not be circularly polarized, and it must not have nulls in the angular region of space over which the test antenna pattern is determined because the probe correction coefficients become infinite.

The measurements are carried out until the signal at the edges of the plane is of very low intensity, usually about 45 dB below the largest signal level within the measuring plane. Defining a and b the width and height, respectively, of the measuring plane, M and N are determined using

$$M = \frac{a}{\Delta x} + 1 \tag{17-10a}$$

$$N = \frac{b}{\Delta y} + 1 \tag{17-10b}$$

The sampling points on the measuring grid are chosen to be less than $\lambda/2$ in order to satisfy the Nyquist sampling criterion. If the plane $z = 0$ is located in the far field of the source, the sample spacings can increase to their maximum value of $\lambda/2$. Usually the rectangular lattice points are separated by the grid spacings of

$$\Delta x = \frac{\pi}{k_{xo}} \tag{17-11a}$$

$$\Delta y = \frac{\pi}{k_{yo}} \tag{17-11b}$$

where k_{xo} and k_{yo} are real numbers and represent the largest magnitudes of k_x and k_y, respectively, such that $\mathbf{f}(k_x, k_y) \simeq 0$ for $|k_x| > k_{xo}$ or $|k_y| > k_{yo}$.

At the grid sample points, the tangential electric field components, E_x and E_y, are recorded. The subscripts x and y represent, respectively, the two polarizations of the probe. The procedure for probe compensation is neglected here. A previously performed characterization of the probe is used to compensate for its directional effects in what is essentially an application of its "transfer function." The electric field components over the entire plane can be reconstructed from the samples taken at the grid points, and each is given by

$$E_{xa}(x, y, z = 0) \simeq \sum_{n=-N/2}^{N/2-1} \sum_{m=-M/2}^{M/2-1} E_x(m\Delta x, n\Delta y, 0)$$
$$\times \frac{\sin(k_{xo}x - m\pi)}{k_{xo}x - m\pi} \frac{\sin(k_{yo}y - n\pi)}{k_{yo}y - n\pi} \tag{17-12a}$$

$$E_{ya}(x, y, z = 0) \simeq \sum_{n=-N/2}^{N/2-1} \sum_{m=-M/2}^{M/2-1} E_y(m\Delta x, n\Delta y, 0)$$
$$\times \frac{\sin(k_{xo}x - m\pi)}{k_{xo}x - m\pi} \frac{\sin(k_{yo}y - n\pi)}{k_{yo}y - n\pi} \tag{17-12b}$$

Using (17-12a) and (17-12b), f_x and f_y of (17-7a) and (17-7b) can be evaluated, using a FFT algorithm, at the set of wavenumbers explicitly defined by the discrete

Fourier transform and given by

$$k_x = \frac{2\pi m}{M \Delta x}, \qquad -\frac{M}{2} \le m \le \frac{M}{2} - 1 \qquad (17\text{-}13a)$$

$$k_y = \frac{2\pi n}{N \Delta y}, \qquad -\frac{N}{2} \le n \le \frac{N}{2} - 1 \qquad (17\text{-}13b)$$

The wavenumber spectrum points are equal to the number of points in the near-field distribution, and the maximum wavenumber coordinate of the wavenumber spectrum is inversely proportional to the near-field sampling spacing. While the maximum sampling spacing is $\lambda/2$, there is no minimum spacing restrictions. However, there are no advantages to increasing the near-field sample points by decreasing the sample spacing. The decreased sample spacing will increase the limits of the wavenumber spectrum points, which are in the large evanescent mode region, and do not contribute to increased resolution of the far-field pattern.

Increased resolution in the far-field power pattern can be obtained by adding artificial data sampling points (with zero value) at the outer extremities of the near-field distribution. This artificially increases the number of sample points without decreasing the sample spacing. Since the sample spacing remains fixed, the wavenumber limits also stay fixed. The additional wavenumber spectrum points are all within the original wavenumber limits and lead to increased resolution in the computed far-field patterns.

To validate the techniques, numerous comparisons between computed far-field patterns, from near-field measurements, and measured far-field patterns have been made. In Figure 17.15, the computed and measured sum and difference far-field azimuth plane patterns for a four-foot diameter parabolic reflector with a nominal gain of 30 dB are displayed [4]. Two measured far-field patterns were obtained on two different high-quality far-field ranges, one at the Georgia Institute of Technology and the other at Scientific-Atlanta. The third trace represents the computed far-field pattern from near-field measurements made at Georgia Tech. There are some minor discrepancies between the two measured far-field patterns which were probably caused by extraneous range reflections. The best agreement is between the computed far-field pattern and the one measured at Scientific-Atlanta. Many other comparisons have been made with similar success. The limited results shown here, and the many others published in the literature [4], [40]–[42] clearly demonstrate the capability of the near-field technique.

The near-field technique provides the antenna designers information not previously available to them. For example, if a given far-field pattern does not meet required specifications, it is possible to use near-field data to pinpoint the cause [43]. Near-field measurements can be applied also to antenna analysis and diagnostic tasks [44], and it is most attractive when efficient near-field data collection and transformation methods are employed.

17.3 RADIATION PATTERNS

The radiation patterns (amplitude and phase), polarization, and gain of an antenna, which are used to characterize its radiation capabilities, are measured on the surface of a constant radius sphere. Any position on the sphere is identified using the standard
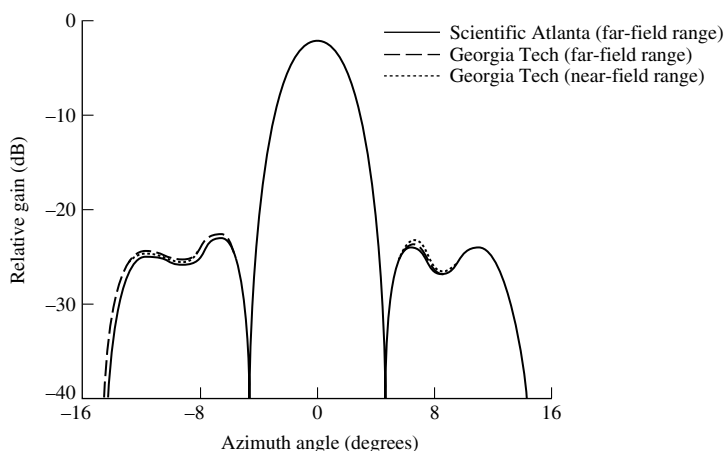
(a) Sum mode
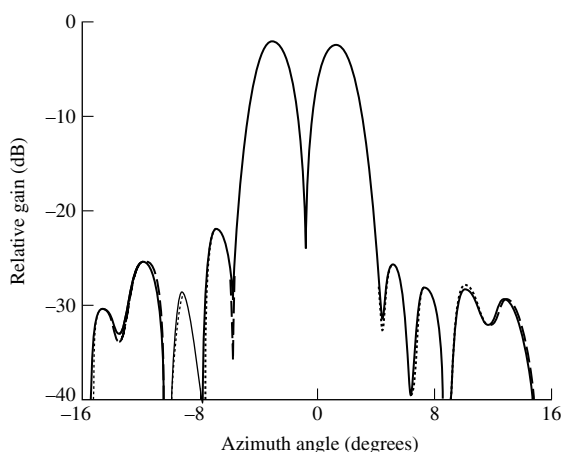
(b) Difference mode

Figure 17.15   Measured and computed sum and difference mode principal-plane far-field patterns for a four-foot parabolic reflector. (SOURCE: E. D. Joy, W. M. Leach, Jr., G. P. Rodrique, and D. T. Paris, "Applications of Probe Compensated Near-Field Measurements," *IEEE Trans. Antennas Propagat.*, Vol. AP-26, No. 3, pp. 379–389, May 1978. © (1978) IEEE)

spherical coordinate system of Figure 17.16. Since the radial distance is maintained fixed, only the two angular coordinates (θ, ϕ) are needed for positional identification. A representation of the radiation characteristics of the radiator as a function of θ and ϕ for a constant radial distance and frequency, is defined as the *pattern* of the antenna.

In general, the pattern of an antenna is three-dimensional. Because it is impractical to measure a three-dimensional pattern, a number of two-dimensional patterns, as defined in Section 2.2, are measured. They are used to construct a three-dimensional pattern. The number of two-dimensional patterns needed to construct faithfully a three-dimensional graph is determined by the functional requirements of the description, and
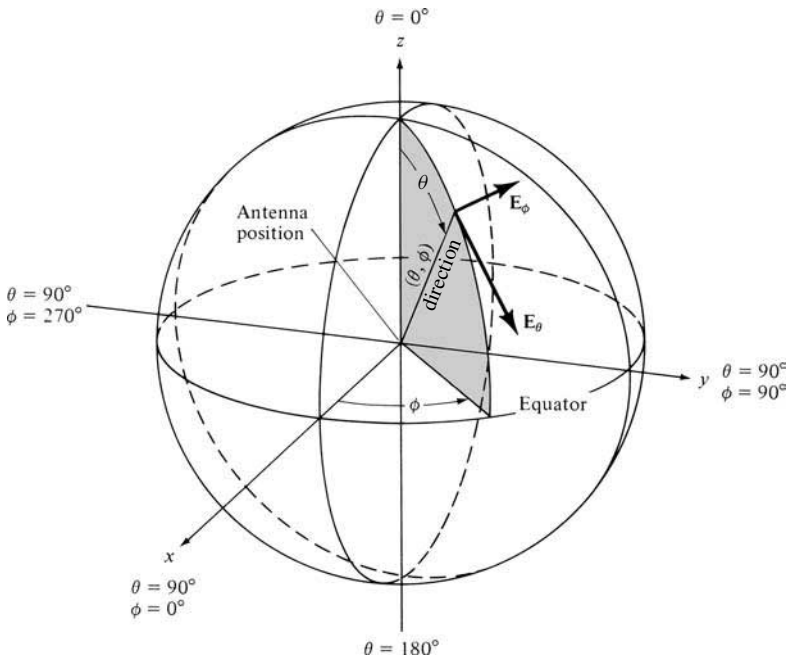
Figure 17.16 Spherical coordinate system geometry. (SOURCE: *IEEE Standard Test Procedures for Antennas*, IEEE Std 149–1979, published by IEEE, Inc., 1979, distributed by Wiley).

the available time and funds. The minimum number of two-dimensional patterns is two, and they are usually chosen to represent the orthogonal principal E- and H-plane patterns, as defined in Section 2.2.

A two-dimensional pattern is also referred to as a *pattern cut*, and it is obtained by fixing one of the angles (θ or ϕ) while varying the other. For example, by referring to Figure 17.16, pattern cuts can be obtained by fixing $\phi_j(0 \leq \phi_j \leq 2\pi)$ and varying $\theta(0 \leq \theta \leq \pi)$. These are referred to as elevation patterns, and they are also displayed in Figure 2.19. Similarly θ can be maintained fixed ($0 \leq \theta_i \leq \pi$) while ϕ is varied ($0 \leq \phi \leq 2\pi$). These are designated as azimuthal patterns. Part ($0 \leq \phi \leq \pi/2$) of the $\theta_i = \pi/2$ azimuthal pattern is displayed in Figure 2.19.

The patterns of an antenna can be measured in the transmitting or receiving mode. The mode is dictated by the application. However, if the radiator is reciprocal, as is the case for most practical antennas, then either the transmitting or receiving mode can be utilized. For such cases, the receiving mode is selected. The analytical formulations upon which an amplitude pattern is based, along with the advantages and disadvantages for making measurements in the transmitting or receiving mode, are found in Section 3.8.2. The analytical basis of a phase pattern is discussed in Section 13.10. Unless otherwise specified, it will be assumed here that the measurements are performed in the receiving mode.

17.3.1 Instrumentation

The instrumentation required to accomplish a measuring task depends largely on the functional requirements of the design. An antenna-range instrumentation must be

designed to operate over a wide range of frequencies, and it usually can be classified into five categories [7]:

1. source antenna and transmitting system
2. receiving system
3. positioning system
4. recording system
5. data-processing system

A block diagram of a system that possesses these capabilities is shown in Figure 17.17.

The source antennas are usually log-periodic antennas for frequencies below 1 GHz, families of parabolas with broadband feeds for frequencies above 400 MHz, and even large horn antennas. The system must be capable of controlling the polarization. Continuous rotation of the polarization can be accomplished by mounting a linearly polarized source antenna on a polarization positioner. Antennas with circular polarization can also be designed, such as crossed log-periodic arrays, which are often used in measurements.

The transmitting RF source must be selected so that it has [7] frequency control, frequency stability, spectral purity, power level, and modulation. The receiving system could be as simple as a bolometer detector, followed possibly by an amplifier, and a
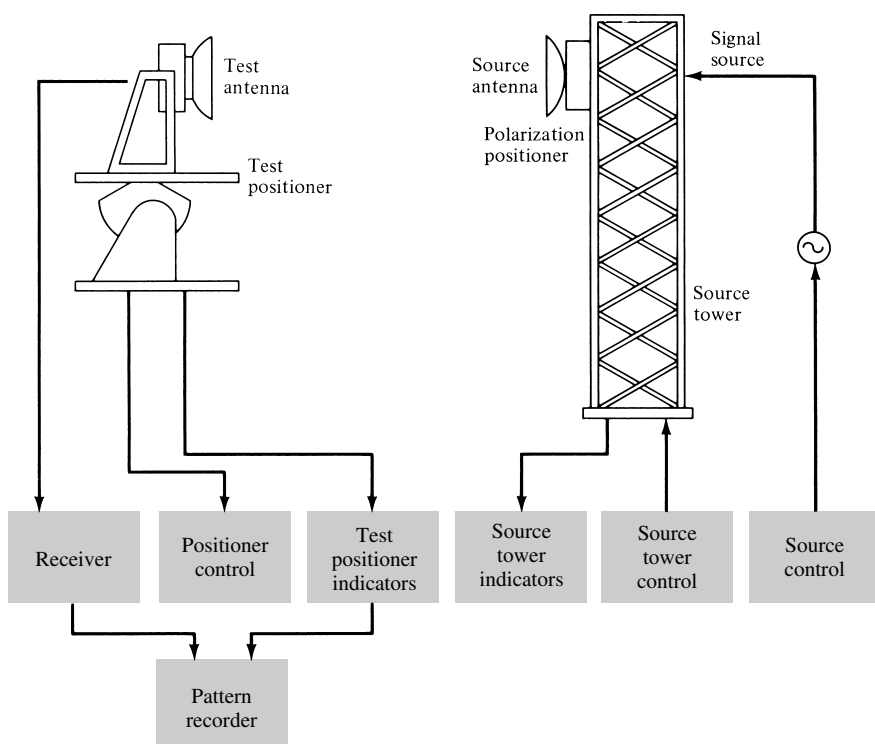

Figure 17.17 Instrumentation for typical antenna-range measuring system. (SOURCE: *IEEE Standard Test Procedures for Antennas*, IEEE Std 149–1979, published by IEEE, Inc., 1979, distributed by Wiley)

recorder. More elaborate and expensive receiving systems that provide greater sensitivity, precision, and dynamic range can be designed. One such system is a heterodyne receiving system [7], which uses double conversion and phase locking, which can be used for amplitude measurements. A dual-channel heterodyne system design is also available [7], and it can be used for phase measurements.

To achieve the desired plane cuts, the mounting structures of the system must have the capability to rotate in various planes. This can be accomplished by utilizing rotational mounts (pedestals), two of which are shown in Figure 17.18. Tower-model elevation-over-azimuth pedestals are also available [7].

There are primarily two types of recorders; one that provides a linear (rectangular) plot and the other a polar plot. The polar plots are most popular because they provide a better visualization of the radiation distribution in space. Usually the recording equipment is designed to graph the relative pattern. Absolute patterns are obtained by making, in addition, gain measurements which will be discussed in the next section. The recording instrumentation is usually calibrated to record relative field or power patterns. Power pattern calibrations are in decibels with dynamic ranges of 0–60 dB. For most applications, a 40-dB dynamic range is usually adequate and it provides sufficient resolution to examine the pattern structure of the main lobe and the minor lobes.

In an indoor antenna range, the recording equipment is usually placed in a room that adjoins the anechoic chamber. To provide an interference free environment, the chamber is closed during measurements. To monitor the procedures, windows or closed-circuit TVs are utilized. In addition, the recording equipment is connected, through

(a) Azimuth–over–elevation positioner   (b) Elevation–over–azimuth positioner
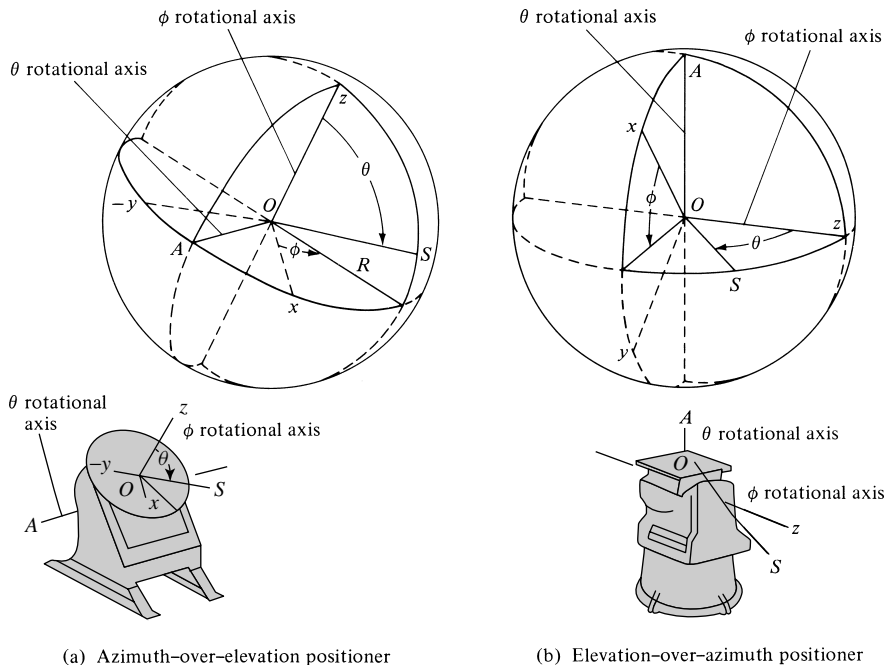
Figure 17.18   Azimuth-over-elevation and elevation-over-azimuth rotational mounts. (SOURCE: *IEEE Standard Test Procedures for Antennas*, IEEE Std 149–1979, published by IEEE, Inc., 1979, distributed by Wiley)
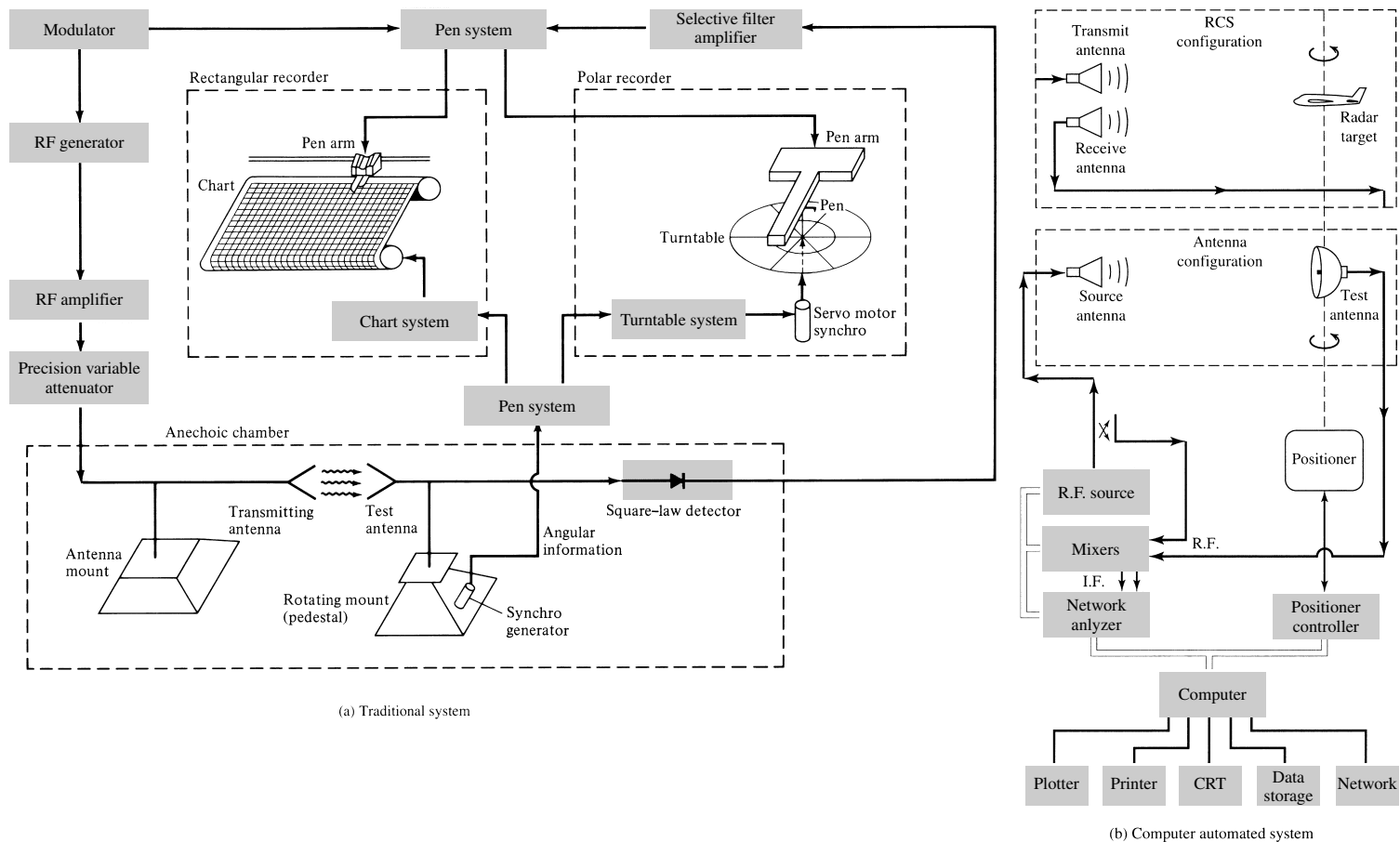
Figure 17.19 Block diagrams of typical instrumentations for measuring rectangular and polar antenna and RCS patterns.

synchronous servo-amplifier systems, to the rotational mounts (pedestals) using the traditional system shown in Figure 17.19(a). The system can record rectangular or polar plots. Position references are recorded simultaneously with measurements, and they are used for angular positional identification. As the rotational mount moves, the pattern is graphed simultaneously by the recorder on a moving chart. One of the axes of the chart is used to record the amplitude of the pattern while the other identifies the relative position of the radiator. A modern configuration to measure antenna and RCS patterns, using a network analyzer and being computer automated, is shown in Figure 17.19(b).

17.3.2   Amplitude Pattern

The total amplitude pattern of an antenna is described by the vector sum of the two orthogonally polarized radiated field components. The pattern on a conventional antenna range can be measured using the system of Figure 17.17 or Figure 17.19 with an appropriate detector. The receiver may be a simple bolometer (followed possibly by an amplifier), a double-conversion phase-locking heterodyne system [7, Fig. 14], or any other design.

In many applications, the movement of the antenna to the antenna range can significantly alter the operational environment. Therefore, in some cases, antenna pattern measurements must be made *in situ* to preserve the environmental performance characteristics. A typical system arrangement that can be used to accomplish this is shown in Figure 17.20. The source is mounted on an airborne vehicle, which is maneuvered through space around the test antenna and in its far-field, to produce a plane wave and to provide the desired pattern cuts. The tracking device provides to the recording equipment the angular position data of the source relative to a reference direction. The measurements can be conducted either by a point-by-point or by a continuous method. Usually the continuous technique is preferred.
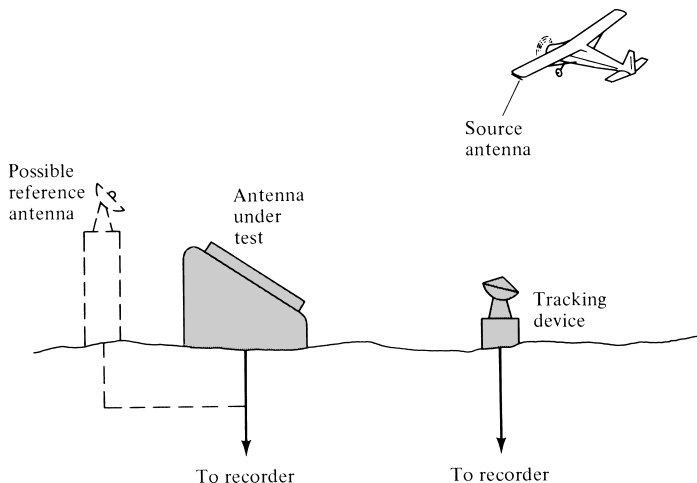

Figure 17.20   System arrangement for *in situ* antenna pattern measurements. (SOURCE: *IEEE Standard Test Procedures for Antennas*, IEEE Std 149–1979, published by IEEE, Inc., 1979, distributed by Wiley)

17.3.3   Phase Measurements

Phase measurements are based on the analytical formulations of Section 13.10. The phase pattern of the field, in the direction of the unit vector $\hat{\mathbf{u}}$, is given by the $\psi(\theta, \phi)$ phase function of (13–63). For linear polarization, $\hat{\mathbf{u}}$ is real, and it may represent $\hat{\mathbf{a}}_\theta$ or $\hat{\mathbf{a}}_\phi$ in the direction of θ or ϕ.

The phase of an antenna is periodic, and it is defined in multiples of $360°$. In addition, the phase is a relative quantity, and a reference must be provided during measurements for comparison.

Two basic system techniques that can be used to measure phase patterns at short and long distances from the antenna are shown respectively, in Figures 17.21(a) and 17.21(b). For the design of Figure 17.21(a), a reference signal is coupled from the transmission line, and it is used to compare, in an appropriate network, the phase of the received signal. For large distances, this method does not permit a direct comparison between the reference and the received signal. In these cases, the arrangement of Figure 17.21(b) can be used in which the signal from the source antenna is received simultaneously by a fixed antenna and the antenna under test. The phase pattern is recorded as the antenna under test is rotated while the fixed antenna serves as a reference. The phase measuring circuit may be the dual-channel heterodyne system [7, Figure 15].

17.4   GAIN MEASUREMENTS

The most important figure of merit that describes the performance of a radiator is the gain. There are various techniques and antenna ranges that are used to measure the gain. The choice of either depends largely on the frequency of operation.
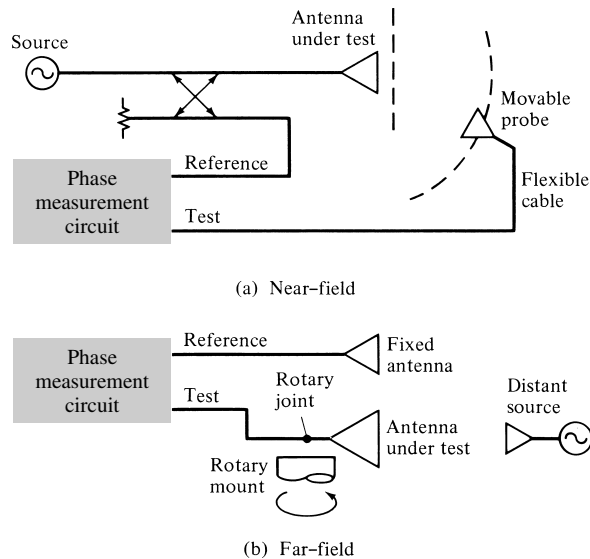

(a) Near–field

(b) Far–field

Figure 17.21   Near-field and far-field phase pattern measuring systems. (SOURCE: *IEEE Standard Test Procedures for Antennas*, IEEE Std 149–1979, published by IEEE, Inc., 1979, distributed by Wiley)

Usually free-space ranges are used to measure the gain above 1 GHz. In addition, microwave techniques, which utilize waveguide components, can be used. At lower frequencies, it is more difficult to simulate free-space conditions because of the longer wavelengths. Therefore between 0.1–1 GHz, ground-reflection ranges are utilized. Scale models can also be used in this frequency range. However, since the conductivity and loss factors of the structures cannot be scaled conveniently, the efficiency of the full scale model must be found by other methods to determine the gain of the antenna. This is accomplished by multiplying the directivity by the efficiency to result in the gain. Below 0.1 GHz, directive antennas are physically large and the ground effects become increasingly pronounced. Usually the gain at these frequencies is measured *in situ*. Antenna gains are not usually measured at frequencies below 1 MHz. Instead, measurements are conducted on the field strength of the ground wave radiated by the antenna.

Usually there are two basic methods that can be used to measure the gain of an electromagnetic radiator: *absolute-gain* and *gain-transfer* (or *gain-comparison*) measurements. The absolute-gain method is used to calibrate antennas that can then be used as standards for gain measurements, and it requires no *a priori* knowledge of the gains of the antennas. Gain-transfer methods must be used in conjunction with standard gain antennas to determine the absolute gain of the antenna under test.

The two antennas that are most widely used and universally accepted as gain standards are the resonant $\lambda/2$ dipole (with a gain of about 2.1 dB) and the pyramidal horn antenna (with a gain ranging from 12–25 dB). Both antennas possess linear polarizations. The dipole, in free-space, exhibits a high degree of polarization purity. However, because of its broad pattern, its polarization may be suspect in other than reflection-free environments. Pyramidal horns usually possess, in free-space, slightly elliptical polarization (axial ratio of about 40 to infinite dB). However, because of their very directive patterns, they are less affected by the surrounding environment.

17.4.1   Absolute-Gain Measurements

There are a number of techniques that can be employed to make absolute-gain measurements. A very brief review of each will be included here. More details can be found in [6]–[8]. All of these methods are based on the Friis transmission formula [as given by (2-118)] which assumes that the measuring system employs, each time, two antennas (as shown in Figure 2.31). The antennas are separated by a distance R, and it must satisfy the far-field criterion of each antenna. For polarization matched antennas, aligned for maximum directional radiation, (2-118) reduces to (2-119).

A. Two-Antenna Method
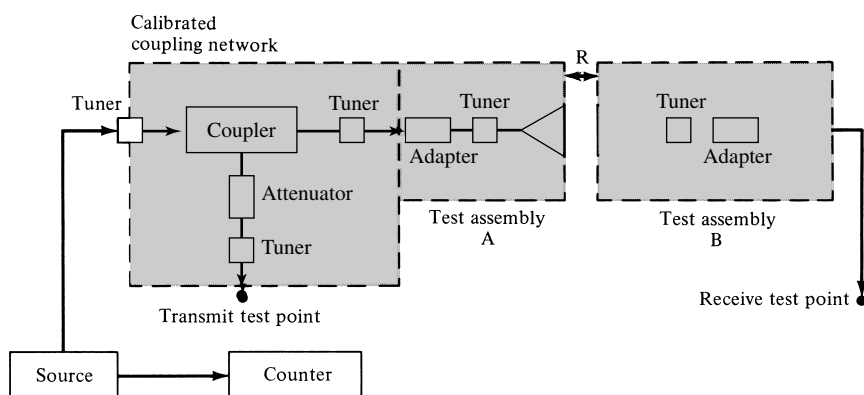Equation (2-119) can be written in a logarithmic decibel form as

$$(G_{0t})_{\text{dB}} + (G_{0r})_{\text{dB}} = 20 \log_{10}\left(\frac{4\pi R}{\lambda}\right) + 10 \log_{10}\left(\frac{P_r}{P_t}\right) \qquad (17\text{-}14)$$
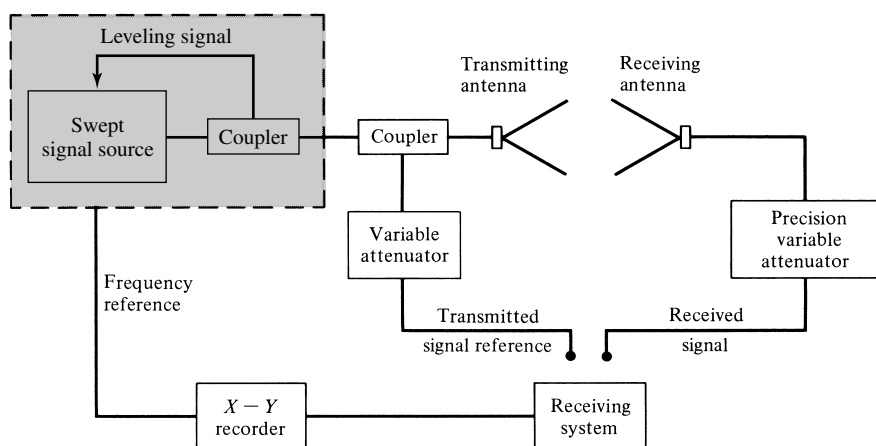
where

$(G_{0t})_{\text{dB}}$ = gain of the transmitting antenna (dB)
$(G_{0r})_{\text{dB}}$ = gain of the receiving antenna (dB)
$\qquad P_r$ = received power (W)

(a) Single frequency

(b) Swept frequency

Figure 17.22 Typical two- and three-antenna measuring systems for single- and swept-frequency measurements. (SOURCE: J. S. Hollis, T. J. Lyon, and L. Clayton, Jr., *Microwave Antenna Measurements*, Scientific-Atlanta, Inc., Atlanta, Georgia, July 1970)

P_t = transmitted power (W)
R = antenna separation (m)
λ = operating wavelength (m)

If the transmitting and receiving antennas are identical ($G_{0t} = G_{0r}$), (17-14) reduces to

$$(G_{0t})_{\text{dB}} = (G_{0r})_{\text{dB}} = \frac{1}{2}\left[20\log_{10}\left(\frac{4\pi R}{\lambda}\right) + 10\log_{10}\left(\frac{P_r}{P_t}\right)\right] \qquad (17\text{-}15)$$

By measuring R, λ, and the ratio of P_r/P_t, the gain of the antenna can be found. At a given frequency, this can be accomplished using the system of Figure 17.22(a). The system is simple and the procedure straightforward. For continuous multifrequency measurements, such as for broadband antennas, the swept-frequency instrumentation of Figure 17.22(b) can be utilized.

B. Three-Antenna Method

If the two antennas in the measuring system are not identical, three antennas (a, b, c) must be employed and three measurements must be made (using all combinations of the three) to determine the gain of each of the three. Three equations (one for each combination) can be written, and each takes the form of (17-14). Thus

(a-b Combination)

$$(G_a)_{\text{dB}} + (G_b)_{\text{dB}} = 20 \log_{10}\left(\frac{4\pi R}{\lambda}\right) + 10 \log_{10}\left(\frac{P_{rb}}{P_{ta}}\right) \qquad (17\text{-}16\text{a})$$

(a-c Combination)

$$(G_a)_{\text{dB}} + (G_c)_{\text{dB}} = 20 \log_{10}\left(\frac{4\pi R}{\lambda}\right) + 10 \log_{10}\left(\frac{P_{rc}}{P_{ta}}\right) \qquad (17\text{-}16\text{b})$$

(b-c Combination)

$$(G_b)_{\text{dB}} + (G_c)_{\text{dB}} = 20 \log_{10}\left(\frac{4\pi R}{\lambda}\right) + 10 \log_{10}\left(\frac{P_{rc}}{P_{tb}}\right) \qquad (17\text{-}16\text{c})$$

From these three equations, the gains $(G_a)_{\text{dB}}$, $(G_b)_{\text{dB}}$, and $(G_c)_{\text{dB}}$ can be determined provided R, λ, and the ratios of P_{rb}/P_{ta}, P_{rc}/P_{ta}, and P_{rc}/P_{tb} are measured.

The two- and three-antenna methods are both subject to errors. Care must be utilized so

1. the system is frequency stable
2. the antennas meet the far-field criteria
3. the antennas are aligned for boresight radiation
4. all the components are impedance and polarization matched
5. there is a minimum of proximity effects and multipath interference

Impedance and polarization errors can be accounted for by measuring the appropriate complex reflection coefficients and polarizations and then correcting accordingly the measured power ratios. The details for these corrections can be found in [7], [8]. There are no rigorous methods to account for proximity effects and multipath interference. These, however, can be minimized by maintaining the antenna separation by at least a distance of $2D^2/\lambda$, as is required by the far-field criteria, and by utilizing RF absorbers to reduce unwanted reflections. The interference pattern that is created by the multiple reflections from the antennas themselves, especially at small separations, is more difficult to remove. It usually manifests itself as a cyclic variation in the measured antenna gain as a function of separation.

C. Extrapolation Method

The extrapolation method is an absolute-gain method, which can be used with the three-antenna method, and it was developed [15] to rigorously account for possible errors due to proximity, multipath, and nonidentical antennas. If none of the antennas used in the measurements are circularly polarized, the method yields the gains and

polarizations of all three antennas. If only one antenna is circularly polarized, this method yields only the gain and polarization of the circularly polarized antenna. The method fails if two or more antennas are circularly polarized.

The method requires both amplitude and phase measurements when the gain and the polarization of the antennas are to be determined. For the determination of gains, amplitude measurements are sufficient. The details of this method can be found in [8], [45].

D. Ground-Reflection Range Method

A method that can be used to measure the gain of moderately broad-beam antennas, usually for frequencies below 1 GHz, has been reported [46]. The method takes into account the specular reflections from the ground (using the system geometry of Figure 17.2), and it can be used with some restrictions and modifications with the two- or three-antenna methods. As described here, the method is applicable to linear antennas that couple only the electric field. Modifications must be made for loop radiators. Using this method, it is recommended that the linear vertical radiators be placed in a horizontal position when measurements are made. This is desired because the reflection coefficient of the earth, as a function of incidence angle, varies very rapidly for vertically polarized waves. Smoother variations are exhibited for horizontally polarized fields. Circularly and elliptically polarized antennas are excluded, because the earth exhibits different reflective properties for vertical and horizontal fields.

To make measurements using this technique, the system geometry of Figure 17.2 is utilized. Usually it is desirable that the height of the receiving antenna h_r be much smaller than the range R_0 ($h_r \ll R_0$). Also the height of the transmitting antenna is adjusted so that the field of the receiving antenna occurs at the first maximum nearest to the ground. Doing this, each of the gain equations of the two- or three-antenna methods take the form of

$$(G_a)_{\text{dB}} + (G_b)_{\text{dB}} = 20 \log_{10} \left(\frac{4\pi R_D}{\lambda} \right) + 10 \log_{10} \left(\frac{P_r}{P_t} \right)$$

$$- 20 \log_{10} \left(\sqrt{D_A D_B} + \frac{r R_D}{R_R} \right) \qquad (17\text{-}17)$$

where D_A and D_B are the directivities (relative to their respective maximum values) along R_D, and they can be determined from amplitude patterns measured prior to the gain measurements. R_D, R_R, λ, and P_r/P_t are also measured. The only quantity that needs to be determined is the factor r which is a function of the radiation patterns of the antennas, the frequency of operation, and the electrical and geometrical properties of the antenna range.

The factor r can be found by first repeating the above measurements but with the transmitting antenna height adjusted so that the field at the receiving antenna is minimized. The quantities measured with this geometry are designated by the same letters as before but with a prime (′) to distinguish them from those of the previous measurement.

By measuring or determining the parameters

1. R_R, R_D, P_r, D_A, and D_B at a height of the transmitting antenna such that the receiving antenna is at the first maximum of the pattern

2. R'_R, R'_D, P'_r, D'_A, and D'_B at a height of the transmitting antenna such that the receiving antenna is at a field minimum

it can be shown [46] that r can be determined from

$$r = \left(\frac{R_R R'_R}{R_D R'_D} \right) \left[\frac{\sqrt{(P_r/P'_r)(D'_A D'_B)} R_D - \sqrt{D_A D_B} R'_D}{\sqrt{(P_r/P'_r)} R_R + R'_R} \right] \qquad (17\text{-}18)$$

Now all parameters included in (17-17) can either be measured or computed from measurements. The free-space range system of Figure 17.22(a) can be used to perform these measurements.

17.4.2 Gain-Transfer (Gain-Comparison) Measurements

The method most commonly used to measure the gain of an antenna is the gain-transfer method. This technique utilizes a gain standard (with a known gain) to determine absolute gains. Initially relative gain measurements are performed, which when compared with the known gain of the standard antenna, yield absolute values. The method can be used with free-space and reflection ranges, and for *in situ* measurements.

The procedure requires two sets of measurements. In one set, using the test antenna as the receiving antenna, the received power (P_T) into a matched load is recorded. In the other set, the test antenna is replaced by the standard gain antenna and the received power (P_S) into a matched load is recorded. In both sets, the geometrical arrangement is maintained intact (other than replacing the receiving antennas), and the input power is maintained the same.

Writing two equations of the form of (17-14) or (17-17), for free-space or reflection ranges, it can be shown that they reduce to [7]

$$(G_T)_{\text{dB}} = (G_S)_{\text{dB}} + 10 \log_{10} \left(\frac{P_T}{P_S} \right) \qquad (17\text{-}19)$$

where $(G_T)_{\text{dB}}$ and $(G_S)_{\text{dB}}$ are the gains (in dB) of the test and standard gain antennas.

System disturbance during replacement of the receiving antennas can be minimized by mounting the two receiving antennas back-to-back on either side of the axis of an azimuth positioner and connecting both of them to the load through a common switch. One antenna can replace the other by a simple, but very precise, $180°$ rotation of the positioner. Connection to the load can be interchanged by proper movement of the switch.

If the test antenna is not too dissimilar from the standard gain antenna, this method is less affected by proximity effects and multipath interference. Impedance and polarization mismatches can be corrected by making proper complex reflection coefficient and polarization measurements [8].

If the test antenna is circularly or elliptically polarized, gain measurements using the gain-transfer method can be accomplished by at least two different methods. One way would be to design a standard gain antenna that possesses circular or elliptical polarization. This approach would be attractive in mass productions of power-gain measurements of circularly or elliptically polarized antennas.

The other approach would be to measure the gain with two orthogonal linearly polarized standard gain antennas. Since circularly and elliptically polarized waves can be decomposed to linear (vertical and horizontal) components, the total power of the wave can be separated into two orthogonal linearly polarized components. Thus the total gain of the circularly or elliptically polarized test antenna can be written as

$$(G_T)_{dB} = 10 \log_{10}(G_{TV} + G_{TH}) \tag{17-20}$$

G_{TV} and G_{TH} are, respectively, the partial power gains with respect to vertical-linear and horizontal-linear polarizations.

G_{TV} is obtained, using (17-19), by performing a gain-transfer measurement with the standard gain antenna possessing vertical polarization. The measurements are repeated with the standard gain antenna oriented for horizontal polarization. This allows the determination of G_{TH}. Usually a single linearly polarized standard gain antenna (a linear $\lambda/2$ resonant dipole or a pyramidal horn) can be used, by rotating it by 90°, to provide both vertical and horizontal polarizations. This approach is very convenient, especially if the antenna possesses good polarization purity in the two orthogonal planes.

The techniques outlined above yield good results provided the transmitting and standard gain antennas exhibit good linear polarization purity. Errors will be introduced if either one of them possesses a polarization with a finite axial ratio. In addition, these techniques are accurate if the tests can be performed in a free-space, a ground-reflection, or an extrapolation range. These requirements place a low-frequency limit of 50 MHz.

Below 50 MHz, the ground has a large effect on the radiation characteristics of the antenna, and it must be taken into account. It usually requires that the measurements are performed on full scale models and *in situ*. Techniques that can be used to measure the gain of large HF antennas have been devised [47]–[49].

17.5   DIRECTIVITY MEASUREMENTS

If the directivity of the antenna cannot be found using solely analytical techniques, it can be computed using measurements of its radiation pattern. One of the methods is based on the approximate expressions of (2-27) by Kraus or (2-30b) by Tai and Pereira, whereas the other relies on the numerical techniques that were developed in Section 2.7. The computations can be performed very efficiently and economically with modern computational facilities and numerical techniques.

The simplest, but least accurate, method requires that the following procedure is adopted:

1. Measure the two principal E- and H-plane patterns of the test antenna.
2. Determine the half-power beamwidths (in degrees) of the E- and H-plane patterns.
3. Compute the directivity using either (2-27) or (2-30b).

The method is usually employed to obtain rough estimates of directivity. It is more accurate when the pattern exhibits only one major lobe, and its minor lobes are negligible.

The other method requires that the directivity be computed using (2-35) where P_{rad} is evaluated numerically using (2-43). The $F(\theta_i, \phi_j)$ function represents the radiation intensity or radiation pattern, as defined by (2-42), and it will be obtained by measurements. U_{max} in (2-35) represents the maximum radiation intensity of $F(\theta, \phi)$ in all space, as obtained by the measurements.

The radiation pattern is measured by sampling the field over a sphere of radius r. The pattern is measured in two-dimensional plane cuts with ϕ_j constant ($0 \leq \phi_j \leq 2\pi$) and θ variable ($0 \leq \theta \leq \pi$), as shown in Figure 2.19, or with θ_i fixed ($0 \leq \theta_i \leq \pi$) and ϕ variable ($0 \leq \phi \leq 2\pi$). The first are referred to as elevation or great-circle cuts, whereas the second represent azimuthal or conical cuts. Either measuring method can be used. Equation (2-43) is written in a form that is most convenient for elevation or great-circle cuts. However, it can be rewritten to accommodate azimuthal or conical cuts.

The spacing between measuring points is largely controlled by the directive properties of the antenna and the desired accuracy. The method is most accurate for broad-beam antennas. However, with the computer facilities and the numerical methods now available, this method is very attractive even for highly directional antennas. To maintain a given accuracy, the number of sampling points must increase as the pattern becomes more directional. The pattern data is recorded digitally on tape, and it can be entered into a computer at a later time. If on-line computer facilities are available, the measurements can be automated to provide essentially real-time computations.

The above discussion assumes that all the radiated power is contained in a single polarization, and the measuring probe possesses that polarization. If the antenna is polarized such that the field is represented by both θ and ϕ components, the *partial directivities* $D_\theta(\theta, \phi)$ and $D_\phi(\theta, \phi)$ of (2-17)–(2-17b) must each be found. This is accomplished from pattern measurements with the probe positioned, respectively, to sample the θ and ϕ components. The *total directivity* is then given by (2-17)–(2-17b), or

$$D_0 = D_\theta + D_\phi \tag{17-21}$$

where

$$D_\theta = \frac{4\pi U_\theta}{(P_{\text{rad}})_\theta + (P_{\text{rad}})_\phi} \tag{17-21a}$$

$$D_\phi = \frac{4\pi U_\phi}{(P_{\text{rad}})_\theta + (P_{\text{rad}})_\phi} \tag{17-21b}$$

U_θ, $(P_{\text{rad}})_\theta$ and U_ϕ, $(P_{\text{rad}})_\phi$ represent the radiation intensity and radiated power as contained in the two orthogonal θ and ϕ field components, respectively.

The same technique can be used to measure the field intensity and to compute the directivity of any antenna that possesses two orthogonal polarizations. Many antennas have only one polarization (θ or ϕ). This is usually accomplished by design and/or proper selection of the coordinate system. In this case, the desired polarization is defined as the *primary polarization*. Ideally, the other polarization should be zero. However, in practice, it is nonvanishing, but it is very small. Usually it is referred to as the *cross polarization*, and for good designs it is usually below −40 dB.

The directivity of circularly or elliptically polarized antennas can also be measured. Precautions must be taken [7] as to which component represents the primary polarization and which the cross-polarization contribution.

17.6   RADIATION EFFICIENCY

The radiation efficiency is defined as the ratio of the total power radiated by the antenna to the total power accepted by the antenna at its input terminals during radiation. System factors, such as impedance and/or polarization mismatches, do not contribute to the radiation efficiency because it is an inherent property of the antenna.

The radiation efficiency can also be defined, using the direction of maximum radiation as reference, as

$$\text{radiation efficiency} = \frac{\text{gain}}{\text{directivity}} \tag{17-22}$$

where directivity and gain, as defined in Sections 2.6 and 2.9, imply that they are measured or computed in the direction of maximum radiation. Using techniques that were outlined in Sections 17.4 and 17.5 for the measurements of the gain and directivity, the radiation efficiency can then be computed using (17-22).

If the antenna is very small and simple, it can be represented as a series network as shown in Figures 2.27(b) or 2.28(b). For antennas that can be represented by such a series network, the radiation efficiency can also be defined by (2-90) and it can be computed by another method [50]. For these antennas, the real part of the input impedance is equal to the total antenna resistance which consists of the radiation resistance and the loss resistance.

The radiation resistance accounts for the radiated power. For many simple antennas (dipoles, loops, etc.), it can be found by analytically or numerically integrating the pattern, relating it to the radiated power and to the radiation resistance by a relation similar to (4-18). The loss resistance accounts for the dissipated power, and it is found by measuring the input impedance (input resistance − radiation resistance = loss resistance).

Because the loss resistance of antennas coated with lossy dielectrics or antennas over lossy ground cannot be represented in series with the radiation resistance, this method cannot be used to determine their radiation efficiency. The details of this method can be found in [50].

17.7   IMPEDANCE MEASUREMENTS

Associated with an antenna, there are two types of impedances: a *self* and a *mutual* impedance. When the antenna is radiating into an unbounded medium and there is no coupling between it and other antennas or surrounding obstacles, the self-impedance is also the driving-point impedance of the antenna. If there is coupling between the antenna under test and other sources or obstacles, the driving-point impedance is a function of its self-impedance and the mutual impedances between it and the other sources or obstacles. In practice, the driving-point impedance is usually referred to as the input impedance. The definitions and the analytical formulations that underlie the self, mutual, and input impedances are presented in Chapter 8.

To attain maximum power transfer between a source or a source-transmission line and an antenna (or between an antenna and a receiver or transmission line-receiver), a conjugate match is usually desired. In some applications, this may not be the most ideal match. For example, in some receiving systems, minimum noise is attained if the antenna impedance is lower than the load impedance. However, in some transmitting systems, maximum power transfer is attained if the antenna impedance is greater

than the load impedance. If conjugate matching does not exist, the power lost can be computed [7] using

$$\frac{P_{\text{lost}}}{P_{\text{available}}} = \left| \frac{Z_{\text{ant}} - Z_{\text{cct}}^*}{Z_{\text{ant}} + Z_{\text{cct}}} \right|^2 \tag{17-23}$$

where

Z_{ant} = input impedance of the antenna

Z_{cct} = input impedance of the circuits which are connected to the antenna at its input terminals

When a transmission line is associated with the system, as is usually the case, the matching can be performed at either end of the line. In practice, however, the matching is performed near the antenna terminals, because it usually minimizes line losses and voltage peaks in the line and maximizes the useful bandwidth of the system.

In a mismatched system, the degree of mismatch determines the amount of incident or available power which is reflected at the input antenna terminals into the line. The degree of mismatch is a function of the antenna input impedance and the characteristic impedance of the line. These are related to the input reflection coefficient and the input VSWR at the antenna input terminals by the standard transmission-line relationships of

$$\frac{P_{\text{refl}}}{P_{\text{inc}}} = |\Gamma|^2 = \frac{|Z_{\text{ant}} - Z_c|^2}{|Z_{\text{ant}} + Z_c|^2} = \left| \frac{\text{VSWR} - 1}{\text{VSWR} + 1} \right|^2 \tag{17-24}$$

where

$\Gamma = |\Gamma| e^{j\gamma}$ = voltage reflection coefficient at the antenna input terminals

VSWR = voltage standing wave ratio at the antenna input terminals

Z_c = characteristic impedance of the transmission line

Equation (17-24) shows a direct relationship between the antenna input impedance (Z_{ant}) and the VSWR. In fact, if Z_{ant} is known, the VSWR can be computed using (17-24). In practice, however, that is not the case. What is usually measured is the VSWR, and it alone does not provide sufficient information to uniquely determine the complex input impedance. To overcome this, the usual procedure is to measure the VSWR, and to compute the magnitude of the reflection coefficient using (17-24). The phase of the reflection coefficient can be determined by locating a voltage maximum or a voltage minimum (from the antenna input terminals) in the transmission line. Since in practice the minima can be measured more accurately than the maxima, they are usually preferred. In addition, the first minimum is usually chosen unless the distance from it to the input terminals is too small to measure accurately. The phase γ of the reflection coefficient is then computed using [51]

$$\gamma = 2\beta x_n \pm (2n - 1)\pi = \frac{4\pi}{\lambda_g} x_n \pm (2n - 1)\pi, \quad n = 1, 2, 3, \ldots \tag{17-25}$$

where

n = the voltage minimum from the input terminals (i.e., $n = 1$ is used to locate the first voltage minimum)

x_n = distance from the input terminals to the nth voltage minimum

λ_g = wavelength measured inside the input transmission line (it is twice the distance between two voltage minima or two voltage maxima)

Once the reflection coefficient is completely described by its magnitude and phase, it can be used to determine the antenna impedance by

$$Z_{\text{ant}} = Z_c \left[\frac{1 + \Gamma}{1 - \Gamma} \right] = Z_c \left[\frac{1 + |\Gamma| e^{j\gamma}}{1 - |\Gamma| e^{j\gamma}} \right] \tag{17-26}$$

Other methods, utilizing impedance bridges, slotted lines, and broadband swept-frequency network analyzers, can be utilized to determine the antenna impedance [51]–[53].

The input impedance is generally a function of frequency, geometry, method of excitation, and proximity to its surrounding objects. Because of its strong dependence on the environment, it should usually be measured *in situ* unless the antenna possesses very narrow beam characteristics.

Mutual impedances, which take into account interaction effects, are usually best described and measured by the cross-coupling coefficients S_{mn} of the device's (antenna's) scattering matrix. The coefficients of the scattering matrix can then be related to the coefficients of the impedance matrix [54].

17.8 CURRENT MEASUREMENTS

The current distribution along an antenna is another very important antenna parameter. A complete description of its amplitude and phase permit the calculation of the radiation pattern.

There are a number of techniques that can be used to measure the current distribution [55]–[58]. One of the simplest methods requires that a small sampling probe, usually a small loop, be placed near the radiator. On the sampling probe, a current is induced which is proportional to the current of the test antenna.

The indicating meter can be connected to the loop in many different ways [55]. If the wavelength is very long, the meter can be consolidated into one unit with the measuring loop. At smaller wavelengths, the meter can be connected to a crystal rectifier. In order not to disturb the field distribution near the radiator, the rectifier is attached to the meter using long leads. To reduce the interaction between the measuring instrumentation and the test antenna and to minimize induced currents on the leads, the wires are wound on a dielectric support rod to form a helical choke. Usually the diameter of each turn, and spacing between them, is about $\lambda/50$. The dielectric rod can also be used as a support for the loop. To prevent a dc short circuit on the crystal rectifier, a bypass capacitor is placed along the circumference of the loop.

There are many other methods, some of them more elaborate and accurate, and the interested reader can refer to the literature [55]–[58].

17.9 POLARIZATION MEASUREMENTS

The polarization of a wave was defined in Section 2.12 as *the curve traced by the instantaneous electric field, at a given frequency, in a plane perpendicular to the direction of wave travel*. The far-field polarization of an antenna is usually measured at
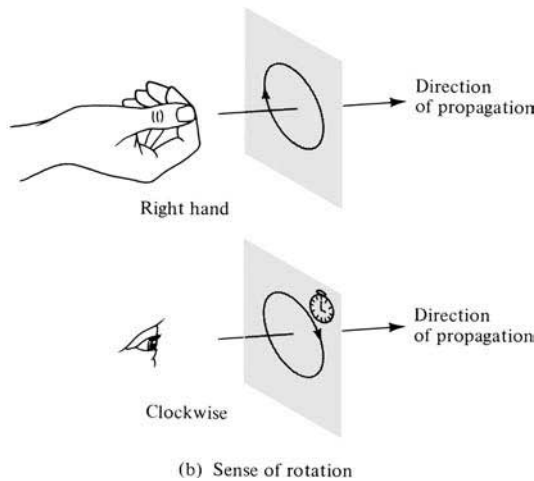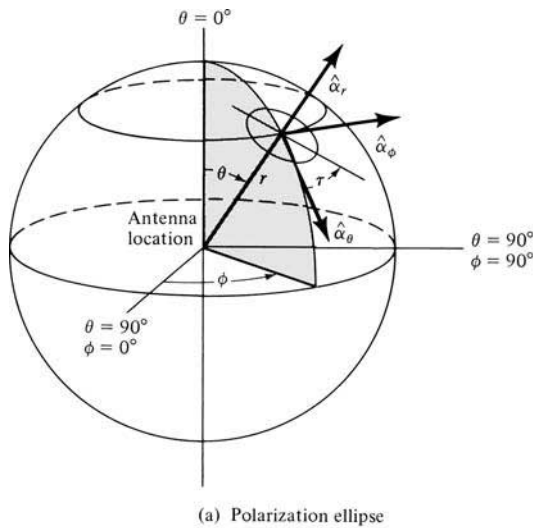
(a) Polarization ellipse

(b) Sense of rotation

Figure 17.23 Polarization ellipse and sense of rotation for antenna coordinate system. (SOURCE: *IEEE Standard Test Procedures for Antennas*, IEEE Std 149–1979, published by IEEE, Inc., 1979, distributed by Wiley)

distances where the field radiated by the antenna forms, in a small region, a plane wave that propagates in the outward radial direction.

In a similar manner, the polarization of the antenna is defined as *the curve traced by the instantaneous electric field radiated by the antenna in a plane perpendicular to the radial direction*, as shown in Figure 17.23(a). The locus is usually an ellipse. In a spherical coordinate system, which is usually adopted in antennas, the polarization ellipse is formed by the orthogonal electric field components of E_θ and E_ϕ. The sense of rotation, also referred to as the sense of polarization, is defined by the sense of rotation of the wave as it is observed along the direction of propagation [see Figure 17.23(b)].

The general polarization of an antenna is characterized by the axial ratio (AR), the sense of rotation (CW or CCW, RH or LH), and the tilt angle τ. The tilt angle is used to identify the spatial orientation of the ellipse, and it is usually measured clockwise from the reference direction. This is demonstrated in Figure 17.23(a) where τ is measured clockwise with respect to $\hat{\mathbf{a}}_\theta$, for a wave traveling in the outward radial direction.

Care must be exercised in the characterization of the polarization of a receiving antenna. If the tilt angle of an incident wave that is polarization matched to the receiving antenna is τ_m, it is related to the tilt angle τ_t of a wave transmitted by the same antenna by

$$\tau_t = 180° - \tau_m \tag{17-27}$$

if a single coordinate system and one direction of view are used to characterize the polarization. If the receiving antenna has a polarization that is different from that of the incident wave, the polarization loss factor (PLF) of Section 2.12.2 can be used to account for the polarization mismatch losses.

The polarization of a wave and/or an antenna can best be displayed and visualized on the surface of a Poincaré sphere [59]. Each polarization occupies a unique point on the sphere, as shown in Figure 17.24. If one of the two points on the Poincaré sphere is used to define the polarization of the incident wave and the other the polarization of the receiving antenna, the angular separation can be used to determine the polarization losses. The procedure requires that the complex polarization ratios of each are determined, and they are used to compute the polarization efficiency in a number of different ways. The details of this procedure are well documented, and they can be found in [7], [8].

Practically it is very difficult to design radiators that maintain the same polarization state in all parts of their pattern. A complete description requires a number of measurements in all parts of the pattern. The number of measurements is determined by the required degree of polarization description.
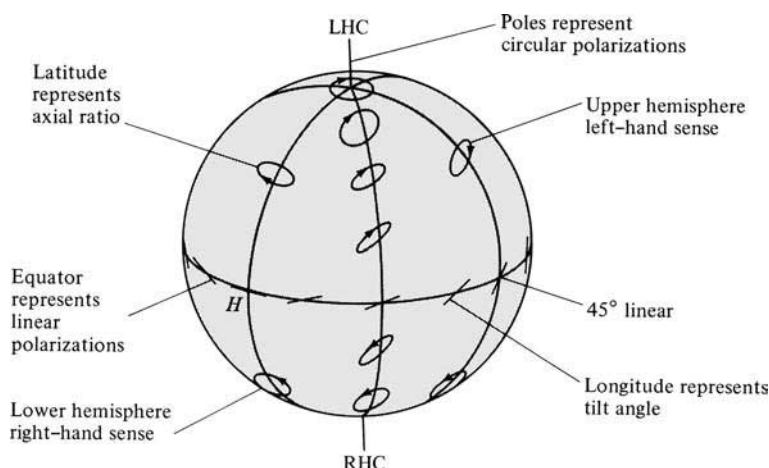

Figure 17.24 Polarization representation on the Poincaré sphere. (SOURCE: W. H. Kummer and E. S. Gillespie, "Antenna Measurements—1978," *Proc. IEEE*, Vol. 66, No. 4, pp. 483–507, April 1978. © (1978) IEEE)

There are a number of techniques that can be used to measure the polarization state of a radiator [7], [8], and they can be classified into three main categories:

1. Those that yield partial polarization information. They do not yield a unique point on the Poincaré sphere.
2. Those that yield complete polarization information but require a polarization standard for comparison. They are referred to as *comparison methods*.
3. Those that yield complete polarization information and require no *a priori* polarization knowledge or no polarization standard. They are designated as *absolute methods*.

The method selected depends on such factors as the type of antenna, the required accuracy, and the time and funds available. A complete description requires not only the polarization ellipse (axial ratio and tilt angle), but also its sense of rotation (CW or CCW, RH or LH).

In this text, a method will be discussed which can be used to determine the polarization ellipse (axial ratio and tilt angle) of an antenna but not its sense of rotation. This technique is referred to as the *polarization-pattern method*. The sense of polarization or rotation can be found by performing auxiliary measurements or by using other methods [7].

To perform the measurements, the antenna under test can be used either in the transmitting or in the receiving mode. Usually the transmitting mode is adopted. The method requires that a linearly polarized antenna, usually a dipole, be used to probe the polarization in the plane that contains the direction of the desired polarization. The arrangement is shown in Figure 17.25(a). The dipole is rotated in the plane of the polarization, which is taken to be normal to the direction of the incident field, and the output voltage of the probe is recorded.

If the test antenna is linearly polarized, the output voltage response will be proportional to $\sin \psi$ (which is the far-zone field pattern of an infinitesimal dipole). The pattern forms a figure-eight, as shown in Figure 17.25(b), where ψ is the rotation angle of the probe relative to a reference direction. For an elliptically polarized test antenna, the nulls of the figure-eight are filled and a dumbbell polarization curve (usually referred to as a *polarization pattern*) is generated, as shown in Figure 17.25(b). The dashed curve represents the polarization ellipse.

The polarization ellipse is tangent to the polarization pattern, and it can be used to determine the axial ratio and the tilt angle of the test antenna. The polarization pattern will be a circle, as shown in Figure 17.25(b), if the test antenna is circularly polarized. Ideally, this process must be repeated at every point of the antenna pattern. Usually it is performed at a number of points that describe sufficiently well the polarization of the antenna at the major and the minor lobes.

In some cases the polarization needs to be known over an entire plane. The axial ratio part of the polarization state can be measured using the arrangement of Figure 17.25(a) where the test probe antenna is used usually as a source while the polarization pattern of the test antenna is being recorded while the test antenna is rotated over the desired plane. This arrangement does not yield the tilt angle or sense of rotation of the polarization state. In order to obtain the desired polarization pattern, the rate of rotation of the linear probe antenna (usually a dipole) is much greater than the rotation rate of the positioner over which the test antenna is mounted and rotated
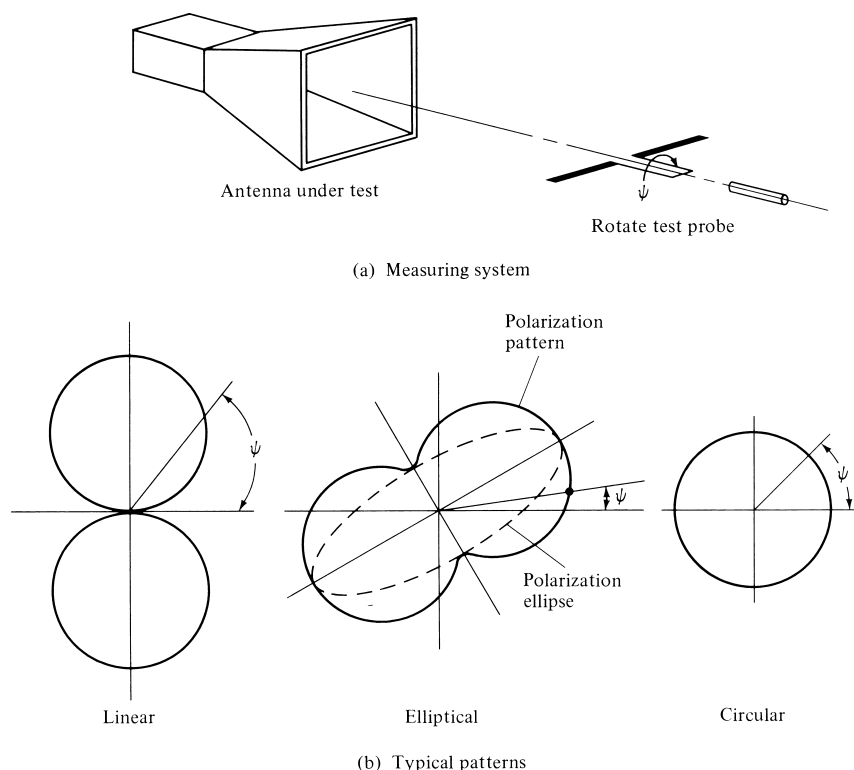
(a) Measuring system

(b) Typical patterns

Figure 17.25   Polarization measuring system and typical patterns.

to allow, ideally, the probe antenna to measure the polarization response of the test antenna at that direction before moving to another angle. When this is performed over an entire plane, a typical pattern recorded in decibels is shown in Figure 17.26 [60], and it is referred as the *axial ratio pattern*. It is apparent that the axial ratio pattern can be inscribed by inner and outer envelopes. At any given angle, the ratio of the outer and inner envelope responses represent the axial ratio. If the pattern is recorded in decibels, the axial ratio is the difference between the outer and inner envelopes (in dB); zero dB difference represents circular polarization (axial ratio of unity). Therefore the polarization pattern of Figure 17.26 indicates that the test antenna it represents is nearly circularly polarized (within 1 dB; axial ratio less than 1.122) at and near $\theta = 0°$ and deviates from that almost monotonically at greater angles (typically by about 7 dB maximum; maximum axial ratio of about 2.24).

The sense of rotation can be determined by performing auxiliary measurements. One method requires that the responses of two circularly polarized antennas, one responsive to CW and the other to CCW rotation, be compared [55]. The rotation sense of the test antenna corresponds to the sense of polarization of the antenna which produced the more intense response.

Another method would be to use a dual-polarized probe antenna, such as a dual-polarized horn, and to record simultaneously the amplitude polarization pattern and the relative phase between the two orthogonal polarizations. This is referred to as the *phase-amplitude* method, and it can be accomplished using the instrumentation of
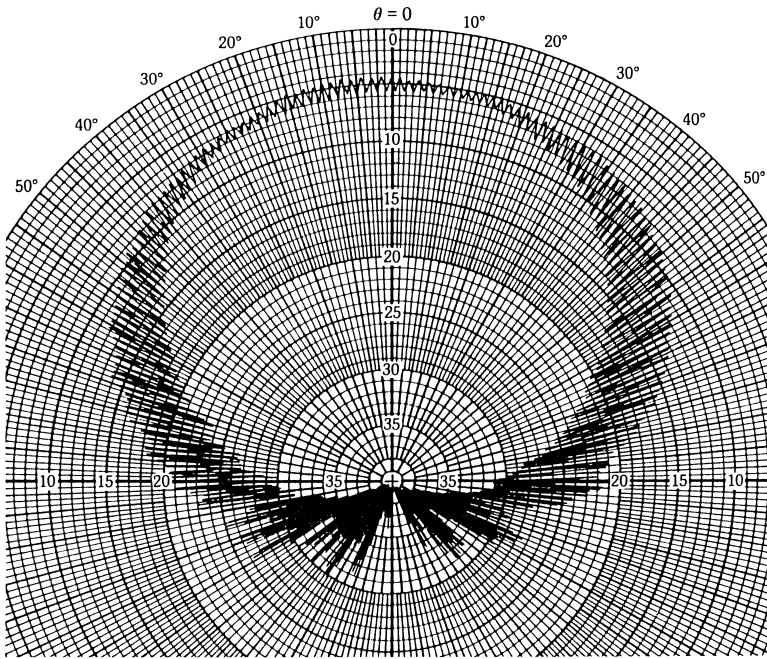
Figure 17.26 Pattern of a circularly polarized test antenna taken with a rotating, linearly polarized, source antenna. (SOURCE: E. S. Gillespie, "Measurement of Antenna Radiation Characteristics on Far-Field Ranges," in *Antenna Handbook* (Y. T. Lo & S. W. Lee, eds.), 1988, © Van Nostrand Reinhold Co., Inc)
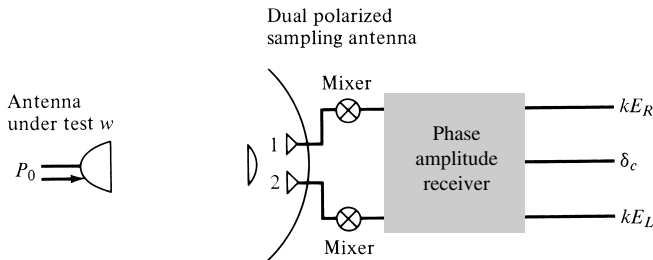

Figure 17.27 System configuration for measurements of polarization amplitude and phase. (SOURCE: W. H. Kummer and E. S. Gillespie, "Antenna Measurements—1978," *Proc. IEEE*, Vol. 66, No. 4, pp. 483–507, April 1978. © (1978) IEEE)

Figure 17.27. Double-conversion phase-locked receivers can be used to perform the amplitude and phase comparison measurements.

Another absolute polarization method, which can be used to completely describe the polarization of a test antenna, is referred to as the *three-antenna* method [7], [8]. As its name implies, it requires three antennas, two of which must not be circularly polarized. There are a number of transfer methods [7], [8], but they require calibration standards for complete description of the polarization state.

17.10   SCALE MODEL MEASUREMENTS

In many applications (such as with antennas on ships, aircraft, large spacecraft, etc.), the antenna and its supporting structure are so immense in weight and/or size that they cannot be moved or accommodated by the facilities of a measuring antenna range. In addition, a movement of the structure to an antenna range can eliminate or introduce environmental effects. To satisfy these system requirements, *in situ* measurements are usually executed.

A technique that can be used to perform antenna measurements associated with large structures is *geometrical scale modeling*. Geometrical modeling is employed to

1. physically accommodate, within small ranges or enclosures, measurements that can be related to large structures;
2. provide experimental control over the measurements;
3. minimize costs associated with large structures and corresponding experimental parametric studies.

Geometrical scale modeling by a factor of n (n smaller or greater than unity) requires the scaling indicated in Table 17.1. The primed parameters represent the scaled model while the unprimed represent the full scale model. For a geometrical scale model, all the linear dimensions of the antenna and its associated structure are divided by n whereas the operating frequency and the conductivity of the antenna material and its structure are multiplied by n. In practice, the scaling factor n is usually chosen greater than unity.

Ideal scale modeling for antenna measurements requires exact replicas, both physically and electrically, of the full scale structures. In practice, however, this is closely approximated. The most difficult scaling is that of the conductivity. If the full scale model possesses excellent conductors, even better conductors will be required in the scaled models. At microwave and millimeter wave frequencies this can be accomplished by utilizing clean polished surfaces, free of films and other residues.

Geometrical scaling is often used for pattern measurements. However, it can also be employed to measure gain, directivity, radiation efficiency, input and mutual impedances, and so forth. For gain measurements, the inability to properly scale the conductivity can be overcome by measuring the directivity and the antenna efficiency

TABLE 17.1   Geometrical Scale Model

Scaled Parameters		Unchanged Parameters	
Length:	$l' = l/n$	Permittivity:	$\epsilon' = \epsilon$
Time:	$t' = t/n$	Permeability:	$\mu' = \mu$
Wavelength:	$\lambda' = \lambda/n$	Velocity:	$v' = v$
Capacitance	$C' = C/n$	Impedance:	$Z' = Z$
Inductance:	$L' = L/n$	Antenna gain:	$G_0' = G_0$
Echo area:	$A_e' = A_e/n^2$		
Frequency:	$f' = nf$		
Conductivity:	$\sigma' = n\sigma$		

and multiplying the two to determine the gain. Scalings that permit additional parameter changes are available [61]. The changes must satisfy the *theorem of similitude*.

REFERENCES

1. J. Brown and E. V. Jull, "The Prediction of Aerial Patterns from Near-Field Measurements," *IEE (London)*, Paper No. 3469E, pp. 635–644, November 1961.

2. R. C. Johnson, H. A. Ecker, and J. S. Hollis, "Determination of Far-Field Antenna Patterns from Near-Field Measurements," *Proc. IEEE*, Vol. 61, No. 12, pp. 1668–1694, December 1973.

3. D. T. Paris, W. M. Leach, Jr., and E. B. Joy, "Basic Theory of Probe-Compensated Near-Field Measurements," *IEEE Trans. Antennas Propagat.*, Vol. AP-26, No. 3, pp. 373–379, May 1978.

4. E. B. Joy, W. M. Leach, Jr., G. P. Rodrigue, and D. T. Paris, "Applications of Probe-Compensated Near-Field Measurements," *IEEE Trans. Antennas Propagat.*, Vol. AP-26, No. 3, pp. 379–389, May 1978.

5. E. F. Buckley, *"Modern Microwave Absorbers and Applications,"* Emerson & Cuming, Inc., Canton, MA.

6. J. S. Hollis, T. J. Lyon, and L. Clayton, Jr., *Microwave Antenna Measurements*, Scientific-Atlanta, Inc., Atlanta, GA, July 1970.

7. *IEEE Standard Test Procedures for Antennas*, IEEE Std 149-1979, Published by IEEE, Inc., 1979, Distributed by Wiley-Interscience.

8. W. H. Kummer and E. S. Gillespie, "Antenna Measurements—1978," *Proc. IEEE*, Vol. 66, No. 4, pp. 483–507, April 1978.

9. L. H. Hemming and R. A. Heaton, "Antenna Gain Calibration on a Ground Reflection Range," *IEEE Trans. Antennas Propagat.*, Vol. AP-21, No. 4, pp. 532–537, July 1973.

10. P. W. Arnold, "The 'Slant' Antenna Range," *IEEE Trans. Antennas Propagat.*, Vol. AP-14, No. 5, pp. 658–659, September 1966.

11. A. W. Moeller, "The Effect of Ground Reflections on Antenna Test Range Measurements," *Microwave Journal*, Vol. 9, pp. 47–54, March 1966.

12. W. H. Emerson, "Electromagnetic Wave Absorbers and Anechoic Chambers Through the Years," *IEEE Trans. Antennas Propagat.*, Vol. AP-21, No. 4, pp. 484–490, July 1973.

13. M. R. Gillette and P. R. Wu, "RF Anechoic Chamber Design Using Ray Tracing," *1977 Int. IEEE/AP-S Symp. Dig.*, pp. 246–252, June 1977.

14. W. H. Emerson and H. B. Sefton, "An Improved Design for Indoor Ranges," *Proc. IEEE*, Vol. 53, pp. 1079–1081, August 1965.

15. J. R. Mentzer, "The Use of Dielectric Lenses in Reflection Measurements," *Proc. IRE*, Vol. 41, pp. 252–256, February 1953.

16. P. A. Beeckman, "Prediction of the Fresnel Region Field of a Compact Antenna Test Range with Serrated Edges," *IEE Proc.*, Vol. 133, Pt. H, No. 2, pp. 108–114, April 1986.

17. H. F. Schluper, "Compact Antenna Test Range Analysis Using Physical Optics," *AMTA Proceedings*, pp. 309–312, Seattle, WA, October 1987.

18. H. F. Schluper, "Verification Method for the Serration Design of CATR Reflectors," *AMTA Proceedings*, pp. 10-9–10-14, Monterey, CA, October 1989.

19. W. D. Burnside, M. C. Gilreath, and B. Kent, "A Rolled Edge Modification of Compact Range Reflectors," Presented at *AMTA Conf.*, San Diego, CA, October 1984.

20. W. D. Burnside, M. C. Gilreath, B. M. Kent, and G. L. Clerici, "Curved Edge Modification of Compact Range Reflector," *IEEE Trans. Antennas Propagat.*, Vol. AP-35, No. 2, pp. 176–182, February 1987.

21. M. R. Hurst and P. E. Reed, "Hybrid Compact Radar Range Reflector," *AMTA Proceedings*, pp. 8-9–8-13, Monterey, CA, October 1989.

22. J. P. McKay and Y. Rahmat-Samii, "Multi-Ring Planar Array Feeds for Reducing Diffraction Effects in the Compact Range," *AMTA Proceedings*, pp. 7-3–7-8, Columbus, OH, October 1992.

23. J. P. McKay, Y. Rahmat-Samii, and F. M. Espiau, "Implementation Considerations for a Compact Range Array Feed," *AMTA Proceedings*, pp. 4-21–4-26, Columbus, OH, October 1992.

24. J. P. McKay and Y. Rahmat-Samii, "A Compact Range Array Feed: Tolerances and Error Analysis," *1993 Int. IEEE/AP-S Symp. Dig.*, Vol. 3, pp. 1800–1803, June 1993.

25. J. P. McKay, Y. Rahmat-Samii, T. J. De Vicente, and L. U. Brown, "An X-Band Array for Feeding a Compact Range Reflector," *AMTA Proceedings*, pp. 141–146, Dallas, TX, October 1993.

26. H. F. Schluper, J. Van Damme, and V. J. Vokurka, "Optimized Collimators—Theoretical Performance Limits," *AMTA Proceedings*, p. 313, Seattle, WA, October 1987.

27. J. D. Huff, J. H. Cook, Jr., and B. W. Smith, "Recent Developments in Large Compact Range Design," *AMTA Proceedings*, pp. 5-39–5-44, Columbus, OH, October 1992.

28. H. F. Schluper and V. J. Vokurka, "Troubleshooting Limitations in Indoor RCS Measurements," *Microwaves & RF*, pp. 154–163, May 1987.

29. V. J. Vokurka, "Seeing Double Improves Indoor Range," *Microwaves & RF*, pp. 71–76, 94, February 1985.

30. T. Harrison, "A New Approach to Radar Cross-Section Compact Range," *Microwave Journal*, pp. 137–145, June 1986.

31. K. W. Lam and V. J. Vokurka, "Hybrid Near-Field/Far-Field Antenna Measurement Techniques," *AMTA Proceedings*, pp. 9-29–9-34, Boulder, CO, October 1991.

32. C. R. Birtcher, C. A. Balanis, and V. J. Vokurka, "RCS Measurements, Transformations, and Comparisons Under Cylindrical and Plane Wave Illumination," *IEEE Trans. Antennas Propagat.*, Vol. AP-42, No. 3, pp. 329–334, March 1994.

33. C. R. Birtcher, C. A. Balanis, and V. J. Vokurka, "Quiet Zone Scan of the Single-Plane Collimating Range," *AMTA Proceedings*, pp. 4-37–4-42, Boulder, CO, October 1991.

34. A. D. Yaghjian, "An Overview of Near-Field Antenna Measurements," *IEEE Trans. Antennas Propagat.*, Vol. AP-34, pp. 30–45, January 1986.

35. P. M. Morse and H. Feshbach, *Methods of Theoretical Physics*, McGraw-Hill, New York, 1953, Chapter 13.

36. A. V. Oppenheim and R. W. Schaffer, *Digital Signal Processing*, Prentice-Hall, Englewood Cliffs, NJ, 1975, Chapter 3.

37. Y. Rahmat-Samii, V. Galindo, and R. Mittra, "A Plane-Polar Approach for Far-Field Construction from Near-Field Measurements," *IEEE Trans. Antennas Propagat.*, Vol. AP-28, No. 3, pp. 216–230, March 1980.

38. L. I. Williams and Y. Rahmat-Samii, "Novel Bi-Polar Planar Near-Field Measurement Scanner at UCLA," 1991 Int. IEEE/AP-S Symp. Dig., London, Ontario, Canada, June 1991.

39. G. D. Bergland, "A Guided Tour of the Fast Fourier Transform," *IEEE Spectrum*, pp. 41–52, July 1969.

40. W. M. Leach, Jr. and D. T. Paris, "Probe Compensated Near-Field Measurements on a Cylinder," *IEEE Trans. Antennas Propagat.*, Vol. AP-21, No. 4, pp. 435–445, July 1973.

41. C. F. Stubenrauch and A. C. Newell, "Some Recent Near-Field Antenna Measurements at NBS," *Microwave J.*, pp. 37–42, November 1980.

42. J. Lemanczyk and F. H. Larsen, "Comparison of Near-Field Range Results," *IEEE Trans. Antennas Propagat.*, Vol. AP-36, No. 6, pp. 845–851, June 1988.

43. J. J. Lee, E. M. Ferren, D. P. Woollen, and K. M. Lee, "Near-Field Probe Used as a Diagnostic Tool to Locate Defective Elements in an Array Antenna," *IEEE Trans. Antennas Propagat.*, Vol. AP-36, No. 6, pp. 884–889, June 1988.

44. Y. Rahmat-Samii and J. Lemanczyk, "Application of Spherical Near-Field Measurements to Microwave Holographic Diagnosis of Antennas," *IEEE Trans. Antennas Propagat.*, Vol. AP-36, No. 6, pp. 869–878, June 1988.

45. A. C. Newell, R. C. Baird, and P. F. Wacker, "Accurate Measurement of Antenna Gain and Polarization at Reduced Distances by an Extrapolation Technique," *IEEE Trans. Antennas Propagat.*, Vol. AP-21, No. 4, pp. 418–431, July 1973.

46. L. H. Hemming and R. A. Heaton, "Antenna Gain Calibration on a Ground Reflection Range," *IEEE Trans. Antennas Propagat.*, Vol. AP-21, No. 4, pp. 532–537, July 1973.

47. R. G. FitzGerrell, "Gain Measurements of Vertically Polarized Antennas over Imperfect Ground," *IEEE Trans. Antennas Propagat.*, Vol. AP-15, No. 2, pp. 211–216, March 1967.

48. R. G. FitzGerrell, "The Gain of a Horizontal Half-Wave Dipole over Ground," *IEEE Trans. Antennas Propagat.*, Vol. AP-15, No. 4, pp. 569–571, July 1967.

49. R. G. FitzGerrell, "Limitations on Vertically Polarized Ground-Based Antennas as Gain Standards," *IEEE Trans. Antennas Propagat.*, Vol. AP-23, No. 2, pp. 284–286, March 1975.

50. E. H. Newman, P. Bohley, and C. H. Walter, "Two Methods for the Measurement of Antenna Efficiency," *IEEE Trans. Antennas Propagat.*, Vol. AP-23, No. 4, pp. 457–461, July 1975.

51. M. Sucher and J. Fox, *Handbook of Microwave Measurements*, Vol. I, Polytechnic Press of the Polytechnic Institute of Brooklyn, New York, 1963.

52. C. G. Montgomery, *Techniques of Microwave Measurements*, Vol. II, MIT Radiation Laboratory Series, Vol. 11, McGraw-Hill, New York, 1947, Chapter 8.

53. ANSI/IEEE Std 148–1959 (Reaff 1971).

54. R. E. Collin, *Foundations for Microwave Engineering*, pp. 248–257, McGraw-Hill, New York, 1992.

55. J. D. Kraus, *Antennas*, McGraw-Hill, New York, 1988.

56. G. Barzilai, "Experimental Determination of the Distribution of Current and Charge Along Cylindrical Antennas," *Proc. IRE (Waves and Electrons Section)*, pp. 825–829, July 1949.

57. T. Morita, "Current Distributions on Transmitting and Receiving Antennas," *Proc. IRE*, pp. 898–904, August 1950.

58. A. F. Rashid, "Quasi-Near-Zone Field of a Monopole Antenna and the Current Distribution of an Antenna on a Finite Conductive Earth," *IEEE Trans. Antennas Propagat.*, Vol. AP-18, No. 1, pp. 22–28, January 1970.

59. H. G. Booker, V. H. Rumsey, G. A. Deschamps, M. I. Kales, and J. I. Bonhert, "Techniques for Handling Elliptically Polarized Waves with Special Reference to Antennas," *Proc. IRE*, Vol. 39, pp. 533–552, May 1951.

60. E. S. Gillespie, "Measurement of Antenna Radiation Characteristics on Far-Field Ranges," Chapter 32 in *Antenna Handbook* (Y. T. Lo and S. W. Lee, eds.), pp. 32-1–32-91, Van Nostrand Reinhold Co., Inc., New York, 1988.

61. G. Sinclair, "Theory of Models of Electromagnetic Systems," *Proc. IRE*, Vol. 36, pp. 1364–1370, November 1948.